This is a non-peer reviewed preprint. Manuscript submitted to Nature Scientific Reports.

Late Holocene relative sea-level records from coral microatolls at Sentosa, Singapore

Fangyi Tan[1,2] *, Benjamin P Horton[1,2], Lin Ke[1**], Tanghua Li[1**], Quye-Sawyer Jennifer[1], Joanne TY Lim[1], Dongju Peng[1], Zihan Aw[1], Shi Jun Wee[2], Jing Ying Yeo[1], Ivan Haigh[3], Xianfeng Wang[1,2], Lin Thu Aung[1], Andrew Mitchell[1], Gina Sarkawi[1,2], Xinnan Li[1], Nurul Syafiqah Tan[1,2], Aron J Meltzner[1,2]

[1] Earth Observatory of Singapore, Nanyang Technological University, 50 Nanyang Avenue, Singapore, 639798, Singapore

[2] Asian School of the Environment, Nanyang Technological University, 50 Nanyang Avenue, Singapore, 639798, Singapore

[3] School of Ocean and Earth Science, University of Southampton, National Oceanography Centre, European Way, Southampton, SO14 3ZH, UK

* Corresponding author: Fangyi Tan (fangyi.tan@ntu.edu.sg, fangyi.tan21@gmail.com, @fangyi2110)

** Both authors contributed equally

Abstract

Late Holocene relative sea-level (RSL) data are important to understand the processes driving RSL change, but there is a lack of precise RSL data from the Sunda Shelf. Here, we produced the first Late Holocene RSL record from coral microatolls at Siloso Point in Sentosa, Singapore, demonstrating for the first time the utility of *Diploastrea heliopora* microatolls as sea-level indicators. We produced 12 sea-level index points and three marine limiting data. The precision of the RSL data (< ± 0.2 m, 2σ, and < ± 26 yrs uncertainties, 95% highest density region), combined with the surface profiles of the coral microatolls, reveal small RSL fluctuations superimposed on a net RSL fall of 0.31 ± 0.18 m between 2.8 kyrs BP and 0.6 kyrs BP, at background rates between -0.1 ± 0.3 mm/yr and -0.2 ± 0.7 mm/yr. There are fluctuations in the rate of RSL fall, with periods of stable (between 2.8 and 2.5 kyrs BP), rising (at ~1.8 kyrs BP) and stable (from 0.8 to 0.6 kyrs BP) RSL. The Siloso RSL record shows good agreement with published, high-quality RSL data within the Sunda Shelf, except at 0.8 kyrs BP when data from Merang, Malaysia indicate a lower RSL lowstand than suggested by the Siloso record. Comparison to a suite of glacial isostatic adjustment (GIA) models indicate preference for lower viscosities in the mantle. However, more high quality and precise Late Holocene RSL data are needed to evaluate the drivers of RSL change in the region, the existence of a regional Late Holocene RSL lowstand, and to better constrain the GIA model parameters for the region.

1. Introduction

Understanding the links between climate and relative sea level (RSL) in the Late Holocene (last 4000 yrs) provides context for future sea-level changes[1–3]. Late Holocene RSL reconstructions have been shown to track global temperature changes associated with the Little Ice Age[2,4,5]. Late Holocene RSL proxy data have also been augmented with tide gauge data to study the time of emergence of modern rates of sea-level rise above pre-industrial background levels[6,7]. As processes such as glacial isostatic adjustment (GIA), ocean dynamics, tectonics and sediment compaction can result in local to regional RSL departures from global mean sea level[8], studies of the global time of emergence and global sea-level variability with Late Holocene climate require a global distribution of RSL records[2,7]. However, the existing global Common Era sea-level databases are based heavily on data from the North Atlantic[2,4,7]. While the addition of more sites to the database, including data from the tropical Pacific, has been shown to make little difference to the global sea-level trend[4,5], the influence of adding data from the Sunda Shelf remains to be tested.

Despite notable attempts to study Late Holocene RSL changes in the Sunda Shelf[9–12], data inconsistencies and large uncertainties in the data make deciphering the drivers of RSL change in the region challenging[13]. The spread of RSL elevations from proxy data in the Malay-Thai Peninsula at any time over the past ~3000 yrs is 3-4 m[14], while the RSL variability predicted by GIA models for the region over this time period can reach ~3 m[15–17], presenting challenges for tuning GIA models. Some studies from the Sunda Shelf suggest RSL of up to 3.4 m below present between ~3 and ~0.5 kyrs BP[11,14,18,19] while others do not[12,20]. Indeed, the published Singapore record exhibits a RSL lowstand in the Late Holocene[14]. However, there are only four sea-level index points (SLIPs) in the past ~3000 yrs, all from peats and muds, in part due to the lack of accommodation space for coastal wetland formation as RSL fell from the highstand[21,22]. These data points have RSL uncertainties of $\pm$ 1 m or more[14] due to the large indicative range (mean tide level, MTL; to highest astronomical tide, HAT) of mangroves in the mesotidal environment of Singapore.

Before the existing Late Holocene RSL data from the Sunda Shelf can be used to infer global mean-sea level changes and constrain GIA models[23,24], more high-precision data are needed to assess the influence of spatially distinct local to regional drivers of RSL[13]. A holistic understanding of the drivers of RSL change within the region has local importance for informing sea-level rise projections and coastal management[13], particularly as the region is home to multiple megacities situated in low-elevation coastal zones[25]. For Singapore, a small island city-state, which has about 30% of its country lying within 5 metres of mean sea level[26], a robust understanding of the mechanisms driving RSL in the region is key to the nation's survival.

Here, we present the first RSL reconstructions from fossil coral microatolls in Singapore – and, to our knowledge, the first RSL reconstruction to use *Diploastrea heliopora* microatolls globally. Coral microatolls are fixed biological indicators whose upward growth is controlled by subaerial exposure at extreme low tides rather than accommodation space[27]. To reconstruct RSL, we surveyed the elevations of fossil microatolls compared to their living counterparts. The coral microatolls in our study grow within a narrower indicative range than mangroves, supplying a vertical precision of $< \pm 0.2$ m (2σ). ^{230}Th dates provided a temporal precision of $\leq \pm 26$ yrs (95% highest density region) in the RSL data. In addition, we used surface profiles of the microatolls to infer sea-level tendencies (i.e., whether RSL rose or fell over time) and to splice two overlapping coral microatoll records. The fossil coral data add to the scarce RSL record in the Late Holocene for Singapore and offer an opportunity to detect centennial-scale fluctuations in RSL that previously could not be resolved given the larger uncertainties and inconsistencies of the existing data. Our coral microatoll record at Siloso shows good agreement with independent RSL records in an updated, quality-controlled database of Late Holocene RSL data from the Sunda Shelf, supporting the use of *Diploastrea heliopora* microatolls as accurate and precise sea-level indicators.

2. Study area

Singapore is located ~700 km from the Sunda megathrust, in the core of the Sunda Shelf that is thought to be tectonically stable[28–31] (Figure 1a). The underlying geology of Singapore was formed as a result of the closure of the Palaeo-Tethys ocean and collision between Sibumasu and Indochina-East Malaya[32,33]. In the western and southern parts of Singapore, folded and faulted Triassic sedimentary rocks of the Jurong and Sentosa Groups can be found, which were formerly the forearc basin of the Sukhothai Arc[32]. Most bedrock faults in Singapore are presumed to have been inactive since the Neogene[33]. However, there is some evidence to suggest slight faulting during the Neogene or Quaternary within the Bedok Formation[33], which is found across the Kallang River Basin (Figure 1b) and in the eastern parts of Singapore[34]. The present-day stress regime is aligned with that which produced the bedrock faults in Singapore[33], suggesting renewed faulting may be possible. Modern-day coseismic subsidence of ~2 cm[35] and post-seismic subsidence of ~2 – 6 mm/yr have been recorded by tide gauges and Global Navigation Satellite System (GNSS) measurements in Singapore following the 2004 Sunda megathrust earthquake in Sumatra[36,37].

Paleo sea-level data since the Last Glacial Maximum (LGM) from the Sunda Shelf suggest rates of sea-level changes in the region have been variable[38]. During the deglacial period, rates of RSL rise doubled from up to 7 ± 5.8 mm/yr after the LGM (~20 kyrs BP) to as much as 15.4 ± 8.2 mm/yr during meltwater-pulse 1A (between ~14.7 and ~14.3 kyrs BP)[28,39–41]. The rapid RSL rise during the deglacial transition flooded the Sunda Shelf and broke the land bridge connecting Singapore to the Riau Islands by ~8 kyrs BP . During the early Holocene, there was a slowdown in the rate of RSL rise between ~8.5 kyrs BP and 7 kyrs BP, associated with the final stages of melting of major ice sheets[14,18,19,43]. Following the cessation of melting, sites within the Sunda Shelf experienced mid-Holocene highstands of variable timing and magnitude[12,16,17,44]. Mangrove sediments from Peninsular Malaysia and Singapore suggest the presence of a RSL lowstand between 1 m and 3.4 m below present at ~1 kyrs BP[9,11,18,19]. In the 20th and 21st centuries, rates of RSL rise in the vicinity of Singapore increased from 0.0 ± 1.6 mm/yr (2σ) between 1915 and 1990 to 1.0 ± 2.1 mm/yr (2σ) between 1990 and 2019[17].

Our study site is located at Siloso Point near the northwestern tip of Sentosa (1.2594°N, 103.8122°E), in the Southern Islands of Singapore (Figure 1). The site is a narrow, free-draining reef ~450 m long and ~80 m wide (Figure 1d), underlain by Upper Triassic interbedded sandstones and mudstones of the Fort Siloso Formation[32]. The Fort Siloso Formation at the study site is offset to the west compared to southern extensions of the same formation along an unnamed fault[33]. A southwest-dipping thrust fault terminates east of the study site[33]. The bedrock geology controls the reef substrate. Fossil *Diploastrea heliopora* microatolls are interspersed with living microatolls (primarily *Porites* sp.) and small isolated scleractinian coral heads near the edge of the reef, which is composed mainly of sandy substrate. Patches of the reef closer to the mudstones are underlain predominantly by mud, and here the reef is colonised by the green algae *Halimeda* sp. All corals in this study are located within ~30 m of the edge of the reef, beyond which the reef drops off to depths of more than 0.8 m below mean low water spring (MLWS) tide. There are no structures suggesting any former ponding along this narrow reef, which could bias the RSL reconstructions high[45]. Spring tidal range based on our portable tide gauge sensor at the site (23 July 2020 to 15 August 2022) is 2.6 m

(Supporting Text S1), similar to that recorded by the nearby Tanjong Pagar Tide Gauge (1.2617°N, 103.8517°E)[46] (Figures 1c & S1).

3. Methods

3.1 Coral microatolls as sea-level indicators

A sea-level indicator is any feature (e.g., fossil coral, archaeological monument) that has a known, quantifiable relationship with the tides (termed the 'indicative meaning'), which can be used to estimate past RSL[47,48]. The indicative meaning comprises an indicative range (the elevation range over which the indicator can be found, with respect to the tides), centred on a central value (also known as the reference water level).

Coral microatolls are fixed biological indicators that grow within the lower intertidal zone[49,50] (Figure 2). Prolonged subaerial exposure at extremely low water levels causes the uppermost parts of the coral to desiccate and die, in what is known as a diedown[27]. During a diedown, coral polyps die to a roughly uniform elevation (known as the highest level of survival, or HLS)[51] (Figures 2a & 2b). Following the extreme low tides, the theoretical HLS rises as low tides get progressively higher again, while the coral microatoll's highest level of growth (HLG) progressively catches up to the lowest annual tides. During this time, if the lowest tides rise more quickly than the corals can grow up, the coral's HLG temporarily decouples from sea level, until it is close enough to the theoretical HLS that a transient sea-level lowering causes a new diedown again[51] (Figure 2). Therefore, the HLG just before a diedown (pre-diedown HLG), or the elevations of the ring crests, provides a filtered record of RSL changes through time; between diedowns, the coral's HLG is limited by its growth rate, rather than sea level[52].

In years when the lowest tides get successively lower each year, a new diedown can be expected to occur each year, producing a cluster of closely-spaced diedowns (Figure 2). The magnitude of a diedown (and thus HLS) can be affected by stochastic non-tidal effects (e.g., oceanographic phenomena like the El Niño-Southern Oscillation and Indian Ocean Dipole, and/or extreme local meteorological events)[51,53]. In contrast, the pre-diedown HLG most closely tracks the non-extreme, astronomically-driven lowest tides superimposed on seasonal oscillations[54] (Figure 2).

The concentric rings of a microatoll are diagnostic features permitting its use as a sea-level indicator; where preserved, they indicate that the microatoll was growing within the lower intertidal zone and was intermittently exposed during extreme low tides[55]. Additionally, the HLGs of successive concentric rings are indicative of sea-level tendencies[56]. A sea-level tendency is traditionally applied to sedimentary indicators and describes an increase or decrease in marine influence[57,58]. Here, we use the terminology specifically to infer the direction of RSL change. Concentric rings (and therefore HLG) that rise radially outwards indicate RSL rise (positive sea-level tendency) over the coral's lifetime, and vice versa, although out-of-sequence rings (termed 'overgrowth') can form during periods of rising RSL (Figure 2 & Figure S2). Successive concentric rings with similar HLG elevations show stable RSL, which we assign as having no sea-level tendency (Figure 2).

We reconstruct RSL from the surface morphologies of the fossil coral microatolls, which provide a filtered record of RSL through time. While traditional methods of slabbing provide greater detail of the RSL changes from year to year[51], analyses of the coral microatoll surface, paired with dates from coral cores, provide sufficient temporal resolution for understanding Late Holocene RSL changes.

3.2 Coral elevations

We surveyed the ring crests (pre-diedown HLG) on all fossil corals and the HLG/HLS of living coral microatolls using a total station or digital level (Supporting Text S2). Performing RSL calculations using the relative elevations of pre-diedown HLG avoids the uncertainties associated with the sensitivity of diedown magnitudes to non-tidal drivers of RSL. All elevations were related to the tides and the national geodetic datum, the Singapore Height Datum (SHD) (Supporting Text S2). The elevations of the living microatolls were compared to tidal datums that were derived directly from the turning points of astronomical tides predicted over an 18.61-year period, corresponding to the Lunar Nodal Cycle[59–61] (Supporting Text S1).

3.3 Coral chronology

We drilled two to three ~15 cm long, ~2 cm diameter cores each from several fossil coral microatolls with concentric rings clearly preserved (SILO F1, SILO F3, SILO F15 and SILO F18) and one to two cores each from fossil corals that were more eroded (SILO F2, SILO F5, SILO F6 and SILO F7) (Figure 3). The cores were drilled vertically downwards into the ring crests.

We visually inspected the cores and subsampled the most pristine portions for ^{230}Th dating, avoiding the discoloured upper sections of the cores[12] (Table 1, Figures 4 & S3). All samples were pre-screened for calcite using powder X-ray diffraction (XRD) and dated using a Neptune Plus multi-collector inductively coupled plasma mass spectrometer (MC-ICP-MS) located at the isotope geochemistry laboratory in the Earth Observatory of Singapore (EOS) and Asian

School of the Environment (ASE), Nanyang Technological University of Singapore (Supporting Text S3). As subsequent RSL calculations are based on the relative elevations of the ring crests, a core-specific age extrapolation was made to the ^{230}Th ages to derive the ages of the ring crests (top of the coral cores) based on the sample depth, growth angles and growth rates (Table 1, Supporting Text S4, Figures S3 & S4). Some of the extrapolated age distributions for the core tops are not normally distributed, so we use the 95% credible interval range of the highest density region of the ^{230}Th age distributions (hereafter, 95% HDR) (Table 1)[62]. Unless otherwise stated, all ages are expressed in yrs 'BP' (before present), where 'present' refers to the year 1950 CE.

3.4 Reconstructing relative sea level from sea-level index points and marine limiting data

We produced SLIPs from the measured ages and elevations of the fossil coral microatolls[12,63–65] (Figure 5). The age component of the SLIPs was derived from the 95th percent highest density region credible interval of the extrapolated age of the core top (Table 1, Supporting Text S4, Figure S4). The vertical component of a SLIP is described by an uncertainty (governed largely by the indicative range of the microatolls) about a central tendency (RSL_j). Here, the indicative range refers to the elevation range of the HLG of living microatolls, relative to the tides[12]. The midpoint of the indicative range is the reference water level[47,66,67].

Ideally, RSL should be determined by comparing the elevation of the fossil coral microatolls to the reference water level of their living counterparts of the same genus at the same site, to avoid site-specific biases in the indicative meaning associated with variable hydrogeologic settings and/or spatial differences in the geoid[56,65]. At Siloso, this was not possible as we did not discover any living equivalents of the fossil *Diploastrea heliopora* microatolls at the site. To overcome this, we applied an adjustment to derive the theoretical reference water level for *Diploastrea heliopora* microatolls (E_{dl}) at Siloso. Different genus of coral microatolls can survive at different elevations due to differential tolerance to subaerial exposure and other environmental parameters[56,68,69]. Accordingly, the adjustment was calculated using observations of the relative elevations of living *Diploastrea heliopora* microatolls and *Porites* sp. microatolls at the nearby Kusu and Semakau Islands – and assumes that there is a systematic difference in the indicative meaning between *Diploastrea heliopora* and *Porites* sp. microatolls at any given site (Supporting Text S5, Figure 1c).

The RSL indicated by each dated sample (or core) is estimated as follows:

$$RSL_j = E_{j,df} - E_{dl} \tag{1}$$

where $E_{j,df}$ is the surveyed surface elevation of the jth coral core.

All uncertainties were added in quadrature to derive the total vertical uncertainty (2σ) for each jth sample ($\varepsilon_{j,total}$) (Supporting Text S6):

$$\varepsilon_{j,total} = \sqrt{\varepsilon_{j,1}^2 + \varepsilon_{j,2}^2 + \varepsilon_{j,3}^2 + \varepsilon_{j,4}^2 + \varepsilon_{j,5}^2 + \varepsilon_{j,6}^2} \tag{2}$$

Additional corrections were made to the RSL component of the SLIPs to account for the following: 1) a systematic offset in the elevations of living HLG, which were surveyed within a year or two after a diedown and more closely approximated HLS, rather than the pre-diedown HLG; and 2) significant erosion on SILO F15 (Supporting Text S7).

Fossil corals that do not have clear concentric rings preserved were used as marine limiting data[45,70] (SILO F2 and SILO F5; Figure S5). RSL for marine limiting data were calculated in the same way as SLIPs, but we represent marine limiting data as T-shaped symbols (Figure 5a).

3.5 Continuous record of RSL

We used cross-sectional profiles of the coral microatolls to uncover sea-level tendencies. We constructed 3D digital surface models of the best-preserved fossil microatolls (SILO F1, SILO F18, SILO F3) using Structure-from-Motion photogrammetry, processed in Agisoft Metashape (Figure 3). Photographs of the fossil corals were taken at the lowest of tides, when the fossil corals were fully subaerially exposed. A digital surface model was also produced for the eroded SILO F15 on the day with the lowest predicted tide between 2020 and 2022 (-1.852 m SHD predicted for the Tanjong Pagar tide gauge on 17 June 2022) when the ring crests of the coral were exposed. However, even at the lowest tides observed on this day (-1.58 m SHD) the low grooves between rings were under water, so only the elevations of the ring crests (which are used to reconstruct RSL) are accurate. All digital surface models were georeferenced using unique features (e.g., screw, end of a crack) that were surveyed on the coral microatolls using the total station. A cross-sectional elevation profile was extracted from each georeferenced digital surface model in QGIS along a radial transect that was selected to best represent the RSL history recorded by the microatoll: we selected the transect to capture the highest number of concentric rings possible while avoiding (to the extent possible) particularly eroded sections of the coral and areas of overgrowth (Figure 3). In our study, we expanded the photogrammetry method of Ref.[71] to estimate not only the magnitude of sea-level changes, but to also produce continuous time-series from the radial transects. We translated the distance along each cross-sectional profile into age estimates using the horizontal (radial) distance between the inner and outer cores and the estimated age difference between the crests of the sampled rings (Figure 4; Supporting Text S8). Each cross-sectional profile can be interpreted as a floating chronology that can be shifted to fit within the modelled age uncertainties of its cores (Figure 5b).

We used the variations in HLG elevation across successive concentric rings on fossil coral microatolls to infer sea-level tendencies. The variability in living HLG observed around individual *Porites* sp. coral microatoll colonies is commonly < 5 cm[50,72], but, to the best of our knowledge, no studies of the HLG variability in living *Diploastrea heliopora* microatolls have been conducted. We applied 15 cm as the threshold to determine sea-level tendencies as that is the largest HLG range observed on the living rim of a given living *Diploastrea heliopora* microatoll in our study (Supporting Document SI2), which we interpret as the natural variability in HLG that can be expected in the absence of any RSL change. HLG variability of < 15 cm was interpreted to indicate stable RSL (no tendency). Coral microatolls with HLG that increases (decreases) radially outwards by more than 15 cm were interpreted as rising (falling) RSL, with positive (negative) sea-level tendency.

3.6 Statistical modelling of RSL

We applied the Errors-In-Variables Integrated Gaussian Process (EIV-IGP) model[73] to the SLIPs to quantify rates of RSL change (Figure 6). The EIV-IGP model is a Bayesian model that inverts magnitudes of RSL from the rates of RSL change and accounts for both the vertical and temporal uncertainties of the data. In this model, RSL is modelled as the integral of the RSL rate process using a Gaussian Process prior on the RSL rates[73]. Temporal uncertainties are accounted for by adopting an Errors-In-Variables framework[74]. We note that the EIV-IGP model does not model marine limiting data.

3.7 Updated Late Holocene RSL database for the Sunda Shelf

To provide context for the Siloso coral microatoll record, we produced an updated Late Holocene RSL database for the interior of the Sunda Shelf following the HOLocene SEA-level variability (HOLSEA) database protocol[75], which builds upon earlier regional databases[13,14] (Supporting Text S9; Supporting Document SI1). All radiocarbon ages were standardised to use the latest IntCal20[76] and Marine20[77] calibration curves. We additionally assessed the quality of data based on their susceptibility to age and/or elevation errors[45].

3.8 Glacial Isostatic Adjustment modelling

The Late Holocene SLIPs were compared to an ensemble of GIA models (Figure 6c). The GIA models comprise the widely used 1D model ICE-6G_C (VM5a)[78] and other models modified from ICE-6G_C (VM5a), changing only one parameter of the ICE-6G_C VM5a each time. The modifications include decreases in the 1D upper and lower mantle viscosities, incorporation of a 3D Earth model[79,80], and delays in the deglaciation histories, which were supported by previous studies from the region[11,14,16]. We also compared the SLIPs with the 2σ uncertainties of the GIA model ensemble predictions from Ref.[17] considering GIA input parameters uncertainties. We did not conduct an iterative search for the optimal ice- and earth-model pairing as our data are restricted to the Late Holocene and provide only limited constraints on GIA models.

4. Results

4.1 Coral elevations

The living *Porites* microatolls at Siloso were found between mean low water spring tide (MLWS) and lowest astronomical tide (LAT) (Figure S6). The weighted mean HLG of *Porites* microatolls at the site is -1.42 $\pm$ 0.04 m SHD or 0.20 $\pm$ 0.04 m above LAT (2σ, standard error of the weighted mean, n = 24).

We observed a systematic inter-genus difference between the living HLG of *Diploastrea heliopora* and *Porites* sp. microatolls at Kusu and Semakau Islands (Figure S6). The reference water level for living *Diploastrea heliopora* microatolls at Siloso, derived by applying the inter-genus difference at Kusu and Semakau Islands to the living HLG of *Porites* sp. microatolls at Siloso, was determined at -1.51 m SHD (Figure 5, Supporting Text S6). The indicative range uncertainty for *Diploastrea heliopora* is represented by the standard deviation of the living HLG across *Diploastrea heliopora* microatolls at Kusu and Semakau Islands ($\pm$ 0.10 m, 2σ) (Supporting Text S6, Figure S6b).

The fossil corals at Siloso were found between -1.5 m and -1.2 m SHD (Table 1, Figure 4). SILO F1, SILO F2, SILO F5, SILO F6 and SILO F7 were the highest fossil corals (found between -1.3 m and -1.2 m SHD), followed by SILO F18 (found at ~-1.4 m SHD). SILO F15 and SILO F3 were the lowest fossil corals at the site, found at -1.5 m SHD.

4.2 Coral chronology

The ages of all fossil corals were in sequence, with the inner cores returning older ages than the outer cores (Figures 4 & S4, Table 1). All replicated subsamples ('B1' and 'B2' samples) yielded similar mean corrected ^{230}Th ages that differed by less than 12 yrs between replicates (Supporting Document SI1, 'U-series' sheet), demonstrating reproducibility. All U-Th dated samples had initial δ^{234}U values with 2σ uncertainties that fell within the 145 $\pm$ 5 ‰ range for modern seawater[81] (Supporting Document SI1). The ages of the RSL data, governed by the extrapolated ages of the core tops, range from ~2.8 to ~0.6 kyrs BP, with uncertainties ranging from $\pm$ 4 to $\pm$ 26 yrs (95% HDR) (Table 2).

4.3 Sea-level index points and marine limiting data

We produced 12 new SLIPs and three marine limiting data points (Table 2, Supporting Document SI1). We demonstrate how we reconstructed RSL with an example for the youngest SLIP, which was sampled from the outer core of SILO F3, the lowest and youngest fossil coral at the Siloso site (Figures 3b & 5). The top of the SILO F3 OUT core was at -1.54 m SHD. We subtracted the reference water level of living *Diploastrea heliopora* at Siloso (-1.51 m SHD) from the elevation of the top of the core to derive the uncorrected RSL of -0.03 m. We subtracted 0.03 m from the RSL to account for the fact that the living HLG surveys were conducted within two years after a diedown (Supporting Text S7), producing a final corrected RSL of -0.06 m (Table 2, Supporting Document SI1). To quantify the vertical uncertainty, we added in quadrature the uncertainty in the offset between the living HLG surveyed and the pre-diedown HLG ($\pm$ 0.02 m, 2σ; Supporting Text S7), the indicative range uncertainty for *Diploastrea heliopora* ($\pm$ 0.10 m, 2σ), the uncertainty associated with determining the indicative range ($\pm$ 0.07 m, 2σ) and the levelling uncertainty ($\pm$ 0.01 m), deriving the total vertical RSL uncertainty of $\pm$ 0.13 m (2σ) (Supporting Document SI1). Here, the indicative range uncertainty ($\pm$ 0.10 m, 2σ) is determined from the standard deviation of the living *Diploastrea heliopora* HLG/HLS measured across Kusu and Semakau Islands. The uncertainty in determining the indicative range ($\pm$ 0.07 m, 2σ) stems from having to relate the living HLG/HLS of *Diploastrea heliopora* to that of *Porites* sp. microatolls to estimate an indicative meaning for living *Diploastrea heliopora* microatolls at the Siloso site (Supporting Text S5 & S6; Supporting Document SI2). We applied an age correction to account for the time it would have taken for the dated sample to grow upwards by 11 cm from the depth it was sampled to the surface (Table 1, Supporting Text S4), deriving a final age of 633 $\pm$ 4 yrs BP, or 1317 $\pm$ 4 CE (Table 2).

The Late Holocene fossil *Diploastrea heliopora* coral microatolls cluster in three age ranges. The oldest microatolls cluster around 2.8 to 2.6 kyrs BP and indicate RSL between 0.06 m and 0.41 m above present (Figure 5a, Table 2). They consist of three corals (SILO F1, SILO F6, SILO F7) that grew within proximity (between 4 m and 40 m) of one another, and which had similar morphologies and elevations (Figure 1d). Of these, SILO F1 was best preserved, with 10 concentric rings inferred from its surface morphology (Figure 3a).

The second group of SLIPs cluster from 1.9 to 1.6 kyrs BP (Figure 5a, Table 2). This age cluster consists of two microatolls (SILO F15 and SILO F18) that also grew close to each other (Figure 1d). The ages suggest that the corals grew coevally during parts of their lifetimes and should therefore have experienced a shared RSL history. Detailed analyses of the coral morphologies reveal that SILO F15 was significantly eroded and a uni-directional RSL uncertainty (+0.08 $\pm$ 0.11 m, 2σ) was added to account for erosion (Supporting Text S7). Together, the SLIPs from the two corals indicate RSL between -0.14 m and 0.28 m above present from 1.9 to 1.6 kyrs BP (Figure 5a).

The youngest SLIPs are from a single coral microatoll (SILO F3), which indicates RSL between -0.18 m and 0.10 m from 0.8 to 0.6 kyrs BP (Figure 5a). Two massive fossil corals (SILO F2 and SILO F5) did not have concentric rings preserved and were interpreted as marine limiting data (Figure 5a). They show that RSL was at least 0.17 m above present at 2.7 kyrs BP and at least 0.13 m to 0.14 m above present from 2.2 to 2.1 kyrs BP.

Two periods of RSL fall are apparent from SLIPs whose respective 1σ uncertainties in RSL do not overlap (Figure 5c). The first occurs between 2.6 kyrs BP and 1.9 kyrs BP. The difference in RSL of the youngest SLIP of SILO F1 (SILO F1 OUT) and the oldest SLIP of SILO F15 (SILO F15 IN) indicates RSL fell by 0.15 ± 0.21 m (2σ), although marine limiting data within this period suggests RSL did not fall below 0.12 m (Figure 5a). The second period of RSL fall occurs between 1.6 and 0.8 kyrs BP. Here, the difference in RSL of the youngest SLIP of SILO F18 (SILO F18 OUT) and the oldest SLIP of SILO F3 (SILO F3 IN) indicates RSL fell by 0.18 ± 0.18 m (2σ).

Together, the SLIPs suggest that Late Holocene RSL at Siloso were stable within ± 0.5 m, although short-lived (decadal to centennial) RSL excursions greater than ± 0.5 m cannot be precluded during the temporal gaps between 2.6 kyrs BP and 1.9 kyrs BP, and between 1.6 kyrs BP and 0.8 kyrs BP. Application of the EIV-IGP model suggests a net, long-term RSL fall of 0.31 ± 0.18 mm between 2.8 kyrs BP and 0.6 kyrs BP, at rates between 0.1 ± 0.3 mm/yr and 0.2 ± 0.7 mm/yr (Figure 6). Our data plot at the lower limit of the GIA model predictions, showing better agreement with modifications of the ICE-6G_C (VM5a) that incorporate lower mantle viscosities (Figure 6c).

4.4 Continuous relative sea level and sea-level tendencies

We supported our understanding of RSL changes with cross-sectional profiles of four coral microatolls with clear concentric-ringed structures (Figures 3, 4 & 5b). Ignoring eroded segments of the profiles, the differences in HLG across the concentric rings of SILO F1 and SILO F3 are small (< 9 cm and < 6 cm, respectively; Figure 4), showing they grew during periods of RSL stability (no tendency). The RSL stability inferred from the surface profiles of SILO F1 and SILO F3 are independently supported by the elevations of their SLIPs, which all overlap at the 2σ level (Figure 5).

In contrast, SILO F18 has concentric rings that rise radially outwards, providing clear signs of RSL rise (positive sea-level tendency) in the earlier part of its lifetime, between 1.78 and 1.73 kyrs BP (from R3 to R2). HLG on SILO F18 steps up radially outwards by 16 cm from R3 to R2, ignoring the higher parts of R2 that are interpreted as overgrowth (Figure 4). In the later period between 1.73 and 1.70 kyrs BP (from R2 to R1), HLG increases by less than or equal to 8 cm. The overgrowth inferred on R1 suggests there are more concentric rings hidden beneath the overgrowth that cannot be observed from the surface. While the presence of overgrowth itself must suggest that RSL had to have risen in the past to form overgrowth (Figures 3d, 4, and S2), the timing of this rise and/or possibility of periods with stable or falling RSL that were masked by the overgrowth cannot be precluded. Therefore, we cannot conclude on the sea-level tendencies during this time. The morphology of SILO F15 had been altered by erosion and similarly cannot supply information on sea-level tendencies (Supporting Text S7).

Together, the coral morphologies and SLIPs illustrate that RSL had fluctuated in the Late Holocene in Singapore (Figures 5b & 5c). Three distinct periods with robust sea-level tendencies were inferred from the coral microatoll surface morphologies: 1) stable RSL (no tendency) from 2.8 to 2.5 kyrs BP; 2) rising RSL at ~1.8 kyrs BP by 0.16 m (positive tendency) and 3) stable RSL from 0.8 to 0.6 kyrs BP (no tendency).

5. Discussion

5.1 Coral microatolls as accurate and precise sea-level indicators

In this paper, we demonstrate, for the first time, the utility of fossil *Diploastrea heliopora* coral microatolls as accurate and precise sea-level indicators. To our knowledge, *Diploastrea heliopora* microatolls have not been used in sea-level studies before; the use of *Porites* sp.

coral microatolls is more common[50,71,72]. Existing studies of *Diploastrea heliopora* commonly revolve around paleoclimate[82–84] or ecology[85–87] and do not make reference to the coral microatoll morphology. Our RSL record from *Diploastrea heliopora* microatolls at Siloso is in agreement with coeval, high-quality SLIPs from the East Coast Malay-Thai Peninsula[11,16] and Riau Islands[12] (Figure 7). The concordance amongst independent records and different types of proxies lends support for the validity of *Diploastrea heliopora* microatolls as sea-level indicators.

As a further test of the robustness of the Siloso RSL record, we applied a more conservative indicative meaning for *Diploastrea heliopora* microatolls: between LAT and mean low water neaps (MLWN). We chose LAT as the lower limit because beneath LAT, the corals would permanently be submerged and will not form the microatoll morphology. The upper limit of MLWN was chosen because that is the level that ensures some degree of seawater replenishment daily, for the corals to survive. Application of the conservative indicative meaning expands the lower bound of the SLIPs downwards by 0.5 m to 0.7 m below present-day sea levels, often beyond the range of coeval SLIPs from the region (Figure S10). The upper bounds of the SLIPs remain mostly unchanged, as the lower limit of the elevation range of living *Diploastrea heliopora* HLG that were surveyed were originally already close to LAT. Importantly, the misfit between the Siloso RSL record and GIA models remains a robust feature that cannot be resolved with a more conservative indicative meaning.

Nonetheless, there is still limited understanding of the indicative meaning of *Diploastrea heliopora* microatolls, in part due to the lower tidal elevation of living *Diploastrea heliopora* microatolls that makes them more challenging to locate in the field than their more commonly studied *Porites* sp. counterparts (Figure S6b). Future research would benefit from an improved understanding of the indicative meaning of *Diploastrea heliopora* microatolls in the study region and elsewhere. *Diploastrea heliopora* corals have been documented throughout the Indo-Pacific[84,88,89], including Singapore[86,90] (Figure S11). They are found to inhabit both lagoonal and more exposed, higher-energy reef settings in atoll islands[91,92], but are also tolerant of high sedimentation rates and turbidity[93,94]. *Diploastrea heliopora* corals also have the ability to occupy both steep and gentle slopes and are resistant to being moved by waves, due to their firm attachment to the basal substrate[95]. Therefore, *Diploastrea heliopora* microatolls should exist in a variety of places across the Sunda Shelf.

We were not limited by the challenges that can typically hinder the use of coral microatolls as accurate and precise sea-level indicators, such as ponding[49,50,56] and erosion[12,49,72]. RSL records from the living and fossil coral microatolls in our study are unlikely to be biased by ponding[49] as the corals are distributed close to the edge of a narrow, free-draining reef, with no evidence of any former ramparts that could have acted as a sill to pond water landwards (Figure 1d). The preservation of overgrowth (out-of-sequence growth that grew during the corals' lifetime; Figure S2) and defined concentric ridges across the fossil coral microatolls indicates limited erosion since the corals' death, except for SILO F15, to which we have applied an erosion correction. We also argue that any changes in tidal range over the Late Holocene at our site are likely to be small. Ref.[51] modelled the LAT at Belitung Island (which is also located in the middle of the Sunda Shelf; Figure 1a) to be less than 10 cm lower than present given a RSL of ~+ 2 m at ~7 kyrs BP. Given that Late Holocene RSL at Siloso is within ± 0.7 m of present-day levels, the effects of changes in tidal range are likely to be smaller, and within error of our RSL reconstructions (which are < 0.2 m). Furthermore, unlike sedimentary indicators that may be subject to sediment compaction over time[96,97], the coral microatolls in our study are not prone to significant lowering as they sit on a consolidated, sandy reef substrate. Given the similar elevations of similarly-aged coral microatolls (SILO F1, SILO F6 and SILO F7 in one generation; SILO F15 and SILO F18 in another generation; Table 1) and the position of all fossil coral microatolls along the edge of the reef, parallel to the reef edge, we infer that the fossil corals are in situ and have not been moved by waves or slumped substrate. While SILO F3 was the only fossil coral microatoll of its elevation and age, we did not find any evidence for tilting that would be suggestive of slumping. Additionally, the agreement of the SILO F3 SLIPs with SLIPs from Merang[9] and Kuantan[16] provide corroborating evidence for the validity of the SILO F3 SLIPs.

The combination of the small indicative range and geomorphic setting of the reef contributed to the high vertical (< ± 0.2 m, 2σ) resolution of our coral microatoll record. The vertical precision of our coral microatoll SLIPs is comparable to other coral microatoll studies in the region, which have RSL uncertainties (2σ) of between ± 0.1 m and ± 0.4 m[12,51,55]. The coral microatolls in this study offer improved precision compared to RSL data from other indicators (e.g., mangrove sediments, emerged oysters, shore platform) in the Sunda Shelf region, which have RSL uncertainties of ± 0.2 m to ± 2.3 m (2σ)[9,11,16,19,20,98] (Figure 7). In Singapore, the existing Late Holocene SLIPs from peats and muds have vertical uncertainties ranging from ± 0.7 m to ± 1.9 m (2σ)[14,18,99,100] (Figure 7).

The *Diploastrea heliopora* microatolls in our study also produced RSL data with accurate and precise ages (< ± 26 yrs, 95% HDR). The initial δ^{234}U ranges all fell within uncertainty of the 145 ± 5 ‰ range for modern seawater, suggesting negligible open system behaviour –

corroborated by the stratigraphic ordering of the ^{230}Th dates (Figure S4). Other coral microatolls in the region that use ^{230}Th dates have similarly small uncertainties of $\pm$ 10 yrs to $\pm$ 66 yrs (2σ)[12,63]. The age uncertainties of our fossil corals are smaller than the radiocarbon-dated Late Holocene RSL data in the region, which range from at least ~ $\pm$ 37 yrs to as much as ~ $\pm$ 1186 yrs (2σ) (Figure 7).

We demonstrate the potential for the surface morphologies of coral microatolls to be used to produce continuous records of RSL and to detect more detailed changes in RSL that are not resolvable within the uncertainty of SLIPs. Traditionally, coral microatoll studies that produce continuous records of RSL rely on the matching of coeval diedowns observed in cross sections within coral microatoll slabs[51,101–103]. While logistical constraints prohibited the retrieval of microatoll slabs in our study, we were still able to combine the records from two microatolls (SILO F15 and SILO F18) by matching a ring boundary common to both corals (Figures 3, 4 & 5b), guided by the tight constraints provided by the ^{230}Th dates. The precision of the ^{230}Th dates greatly restricted how much the SILO F15 and SILO F18 derived age-elevation profiles could be shifted to align their coeval diedowns while still fitting within the age constraints of all dated samples. Similar ‘wiggle-matching’ of corals with overlapping ages has been done in paleo-environmental studies by matching the δ^{18}O signatures of coeval corals[104]. However, to our knowledge, the use of surface morphologies to splice together coral records has yet to be applied to RSL reconstructions[105]. With less eroded corals, the details provided by the surface morphologies of the coral microatolls may provide enough information for such ‘wiggle-matching’ to be possible even in the absence of precise ^{230}Th ages. We suggest that this ‘wiggle-matching’ approach could be the solution to producing temporally high-resolution, continuous RSL records, particularly when accurate ^{230}Th ages are challenging to obtain due to the presence of relatively large amounts of non-radiogenic ^{230}Th, open-system behaviour or diagenesis[106,107]. *Diploastrea heliopora* coral microatolls provide an added advantage in that their longevity and slow growth rates (~ 2- 6 mm/yr)[84,91,108] enable longer continuous records of RSL compared to *Porites* sp. fossil corals of comparable sizes[82,86].

5.2 Late Holocene RSL in the Sunda Shelf

We produced a new high-resolution Late Holocene record from Singapore, which spans a time period when data from Singapore are lacking[14] (Figure 7). The SLIPs in our study indicate a net fall in RSL since 2.8 kyrs BP, with long-term rates of RSL change between -0.1 ± 0.3 mm/yr and -0.2 ± 0.7 mm/yr (Figure 6). A Late Holocene RSL fall from a highstand in equatorial locations such as Singapore is commonplace[14,15,109] due to continental levering and ocean syphoning[17,110,111].

The Late Holocene SLIPs from Singapore fall below the GIA model predictions of the ICE-6G_C (VM5a) (by ~0.8 m at 2.8 kyrs BP) (Figure 6c). Decreasing the lower mantle viscosity (from ~2.6×10^{21} Pa s) to 1.0×10^{21} Pa s improves the fit and reduce this misfit by 50% to ~0.4 m at 2.8 kyrs BP. Decreasing the upper mantle viscosity (from 5.0×10^{20} Pa s) to 1.0×10^{20} Pa s improves the fit even more, producing GIA predictions that marginally match the SLIPS. A preference for low upper mantle viscosity was similarly suggested by a previous GIA study using RSL data from far field regions[23]. In contrast, incorporation of a 3D Earth structure, both in the upper and lower mantle, enlarges the data-model misfit. This might be because the 1D background viscosity within the VM5a (e.g., 5.0×10^{20} Pa s in the upper mantle) is too high, such that the addition of a 3D structure would deteriorate the fit. Interestingly, delays in deglaciation histories did not improve model fit in the Late Holocene (as was suggested by published studies in the region for the early to mid Holocene[11,14,16]). Although delaying the ice melting reduces the magnitude of the mid-Holocene highstand[17], it slightly enlarges the misfit with the Late Holocene SLIPs in this study (Figure 6c). This indicates that a simple delay in the deglaciation history (i.e., ice-equivalent sea level) is insufficient, and refinements to the deglaciation rates of ice sheets are necessary to achieve better fit with the Late Holocene data[112]. Indeed, Late Holocene ice-equivalent sea-level changes are still debated[15,23,113]. There is growing evidence of short-term ice-mass fluctuations during the Late Holocene[114–119], which should manifest as a change in RSL in far-field locations[120,121].

Given that the Late Holocene SLIPs at Siloso only marginally intersect the lower bound of the 2σ uncertainty range of the GIA model predictions from Ref.[17], it is possible that the SLIPs were influenced by other local to regional (non-GIA) processes that would have shifted the SLIPs lower. Ref.[122] estimated rates of subsidence between 0.06 and 0.19 mm/yr in the Singapore Straits since the beginning of the Last Interglacial. Similarly, Ref.[123] inferred slow subsidence between 0.2 to 0.3 mm/yr but for the entire Sunda Shelf over the Pleistocene. If we assume 0.2 to 0.3 mm/yr of subsidence over the past 2.8 kyrs BP[123] and correct for this, the SLIPs in our record would be shifted upwards by up to ~0.84 m at 2.8 kyrs BP, reducing the amount of misfit with the ICE-6G_C (ANU-ICE) model from 0.89 m (1.22 m) to 0.05 m (0.38 m). Ref.[124] inferred modern (2014 – 2020) vertical land motion rates of between -4 and 0.5 mm/yr across Singapore using InSAR, but it is unclear if such rates are influenced by far-field effects of seismic ruptures along the Sunda megathrust[35–37].

Previously, Ref.[13] noted inconsistencies within data from the Malay-Thai Peninsula, highlighting the possibility of reworking and sediment compaction as reasons for the discrepancies between the data. In this study, we applied quality control criteria to account for the above, categorising data points as high or low quality[45]. The update to the database resolves most of the data inconsistencies within the region (Figure 7). The two SLIPs derived from mangrove sediments from West Coast Malay-Thai Peninsula[19] and existing Late Holocene SLIPs from Singapore[18,99], which were previously used to suggest regional Late Holocene lowstands up to 3 m below present[14], are now classified as low quality due to the uncertain degree of post-depositional lowering from sediment compaction, possible age contamination, and a lack of evidence to support the provenance of the mangrove sediments (Supporting document SI1; Supporting Text S9).

However, the high-quality SLIPs from East Coast Malay-Thai Peninsula[11] still suggest a RSL lowstand up to 1.3 m below present between 1.6 kyrs BP and 0.9 kyrs BP. At 0.8 kyrs BP, the SLIPs from Merang[11] plot between 0.1 and 1.4 m below the Siloso SLIP, or up to 1.3 m beneath the Siloso SLIP if we assume the conservative indicative meaning for *Diploastrea heliopora* microatolls of LAT to MLWN (Figures 7 & S10). We note that in Ref.[11], the amount of sediment compaction used to correct the SLIPs for post-depositional lowering of the peats is assumed, rather than modelled using mechanical decompaction models[96,125], so it is possible that the amount of post-depositional lowering was underestimated. Nonetheless, due to the scarcity of high-quality SLIPs from Siloso and other sites within the region during this time (Figure 7), we cannot conclude on the presence or absence of a RSL lowstand until more high-resolution, high-quality SLIPs are produced.

Conclusion

We have produced the first RSL record from fossil *Diploastrea heliopora* coral microatolls in Siloso, Singapore, comprising 12 SLIPs and three marine limiting data points. The RSL record has high vertical (< ± 0.2 m, 2σ) and temporal (< ± 26 yrs, 95% HDR) precision. The SLIPs and marine limiting data, combined with the surface profiles of the coral microatolls, were used to infer sea-level tendencies and continuous RSL changes over the corals' lifetimes. We find a net Late Holocene RSL fall of 0.31 ± 0.18 m between 2.8 kyrs BP and 0.6 kyrs BP, with background rates between -0.1 ± 0.3 mm/yr and -0.2 ± 0.7 mm/yr. Superimposed on the long-term fall in Late Holocene RSL are slight fluctuations, with periods of stable (between 2.8 and 2.5 kyrs BP), rising (at ~1.8 kyrs BP) and stable (from 0.8 to 0.6 kyrs BP) RSL.

The Late Holocene RSL record at Siloso mostly agrees well with published high-quality RSL data derived from peats and muds within the region, demonstrating for the first time the utility of *Diploastrea heliopora* microatolls as accurate and precise sea-level indicators. However, data from Merang, Malaysia indicate a lower RSL lowstand at 0.8 kyrs BP than that suggested by the Siloso RSL record. Comparison of the Siloso RSL record with a GIA model ensemble indicates preference for lower mantle viscosities, although more high-quality and precise RSL records are needed to better constrain the GIA model parameters for the region and to assess the presence and nature of a Late Holocene RSL lowstand.

Author contributions

Fangyi Tan: conceptualisation, methodology, formal analysis, field and laboratory data processing, writing – original draft, revised draft. Benjamin P Horton: conceptualisation, writing – reviewing and editing. Lin Ke: laboratory methods and analyses of U-Th dates, writing – reviewing and editing. Tanghua Li: glacial isostatic adjustment modelling methods, writing – reviewing and editing. Jennifer Quye-Sawyer: analyses of U-Th dates, writing – reviewing and editing. Joanne TY Lim: processing of elevation and tide gauge data, fieldwork, writing – reviewing and editing. Dongju Peng: local tidal model, writing – reviewing and editing. Zihan Aw: processing of elevation and tide gauge data, fieldwork, writing – reviewing and editing. Shi Jun Wee: processing of coral digital surface models, fieldwork, writing – reviewing and editing. Andrew Mitchell: processing of elevation data, fieldwork, writing – reviewing and editing. Jing Ying Yeo: processing of X-ray diffraction data, fieldwork, writing – reviewing and editing. Ivan Haigh: tidal datum calculation methods, writing – reviewing and editing. Xianfeng Wang: spike preparation and analyses of U-Th dates, writing – reviewing and editing. Lin Thu Aung, Gina Sarkawi, Xinnan Li, Nurul Syafiqah Tan: fieldwork, writing – reviewing and editing. Aron J Meltzner: conceptualisation, supervision, funding acquisition, writing – reviewing and editing.

Declaration of competing interests

The authors declare that they have no known competing financial interests or personal relationships that could have appeared to influence the work reported in this paper.

Acknowledgements

Funding for this work came from the National Research Foundation Singapore under its Singapore NRF Fellowship scheme (Award NRF-NRFF11-2019-0008 to A.J.M.), and the Ministry of Education, Singapore, under its Singapore Ministry of Education Academic Research Fund (Award MOE2019-T3-1-004 to B.P.H. and A.J.M., Award MOE-T2EP50120-0007 to B.P.H., and Award MOE-T2EP10122-0006 to X.W.). This research was conducted under the Singapore National Parks Board research permit NP/RP20-122-2a, with support of the Sentosa Development Corporation team, particularly G. Lee, L. Tan, and the Sentosa environmental management team.

We are grateful for the help of many colleagues in field data collection, laboratory and data processing and figure improvements, including P.S. Aung, J.A. Encillo, C. Sundod and team from the Centre of Geohazards Observations, led by C.Y. Leong; B. Perttu; S.F. Wee; D.W. Huang; D. Lallemant; and M.H. Ikhsan. The GIA modelling is conducted in part with services offered by Information Technology Services at the University of Hong Kong. This is Earth Observatory of Singapore contribution no. 560.

Data availability

The data will be made available with the published manuscript.

References

1. Barnett, R. L., Kemp, A. C. & Gehrels, W. R. Late Holocene sea level. *PAGES Mag* **27**, (2019).
2. Kopp, R. E. *et al.* Temperature-driven global sea-level variability in the Common Era. *Proc. Natl. Acad. Sci. U.S.A.* **113**, (2016).
3. Nidheesh, A. G., Lengaine, M., Vialard, J., Unnikrishnam, A. S. & Dayan, H. Decadal and long-term sea level variability in the tropical Indo-Pacific Ocean. *Climate Dynamics* **41**, 381–402 (2013).
4. Kemp, A. C. *et al.* Relative sea-level change in Newfoundland, Canada during the past ∼3000 years. *Quaternary Science Reviews* **201**, 89–110 (2018).
5. Walker, J. S. *et al.* Common Era sea-level budgets along the U.S. Atlantic coast. *Nat Commun* **12**, 1841 (2021).
6. Gehrels, R. & Woodworth, P. L. When did modern rates of sea-level rise start? *Global and Planetary Change* **100**, 263–277 (2013).

7. Walker, J. S., Kopp, R. E., Little, C. M. & Horton, B. P. Timing of emergence of modern rates of sea-level rise by 1863. *Nat Commun* **13**, 966 (2022).

8. Horton, B. P. *et al.* Mapping Sea-Level Change in Time, Space, and Probability. *Annu. Rev. Environ. Resour.* **44**, 481–521 (2018).

9. Kamaludin, H., Akmal, S., Minerals & Geoscience Department Malaysia, Zong, Y., & Department of Earth Sciences, University of Hong Kong. Late Holocene relative low sea level at Merang, Terengganu. *BGSM* **62**, 23–29 (2016).

10. Scheffers, A. *et al.* Holocene sea levels along the Andaman Sea coast of Thailand. *The Holocene* **22**, 1169–1180 (2012).

11. Tam, C.-Y. *et al.* A below-the-present late Holocene relative sea level and the glacial isostatic adjustment during the Holocene in the Malay Peninsula. *Quaternary Science Reviews* **201**, 206–222 (2018).

12. Wan, J. X. W. *et al.* Relative sea-level stability and the radiocarbon marine reservoir correction at Natuna Island, Indonesia, since 6400 yr BP. *Marine Geology* **430**, 106342 (2020).

13. Mann, T. *et al.* Holocene sea levels in Southeast Asia, Maldives, India and Sri Lanka: The SEAMIS database. *Quaternary Science Reviews* **219**, 112–125 (2019).

14. Chua, S. *et al.* A new Holocene sea-level record for Singapore. *The Holocene* **31**, 1376–1390 (2021).

15. Bradley, S. L., Milne, G. A., Horton, B. P. & Zong, Y. Modelling sea level data from China and Malay-Thailand to estimate Holocene ice-volume equivalent sea level change. *Quaternary Science Reviews* **137**, 54–68 (2016).

16. Zhang, Y. *et al.* The middle-to-late Holocene relative sea-level history, highstand and levering effect on the east coast of Malay Peninsula. *Global and Planetary Change* **196**, 103369 (2021).
17. Li, T. *et al.* Glacial Isostatic Adjustment modelling of the mid-Holocene sea-level highstand of Singapore and Southeast Asia. *Quaternary Science Reviews* **319**, 108332 (2023).
18. Bird, M. I. *et al.* Punctuated eustatic sea-level rise in the early mid-Holocene. *Geology* **38**, 803–806 (2010).
19. Geyh, M. A., Streif, H. & Kudrass, H.-R. Sea-level changes during the late Pleistocene and Holocene in the Strait of Malacca. *Nature* **278**, 441–443 (1979).
20. Tjia, H. D., Fujii, S. & Kigoshi, K. Holocene shorelines of Tioman island in the south China sea. *Geol. Mijnbouw* **62**, 599–604 (1983).
21. Dura, T. *et al.* The Role of Holocene Relative Sea-Level Change in Preserving Records of Subduction Zone Earthquakes. *Curr Clim Change Rep* **2**, 86–100 (2016).
22. Kelsey, H. M. *et al.* Accommodation space, relative sea level, and the archiving of paleo-earthquakes along subduction zones. *Geology* **43**, 675–678 (2015).
23. Lambeck, K., Rouby, H., Purcell, A., Sun, Y. & Sambridge, M. Sea level and global ice volumes from the Last Glacial Maximum to the Holocene. *Proc. Natl. Acad. Sci. U.S.A.* **111**, 15296–15303 (2014).
24. Peltier, W. R. On eustatic sea level history: Last Glacial Maximum to Holocene. *Quaternary Science Reviews* **21**, 377–396 (2002).
25. Neumann, B., Vafeidis, A. T., Zimmermann, J. & Nicholls, R. J. Future Coastal Population Growth and Exposure to Sea-Level Rise and Coastal Flooding - A Global Assessment. *PLoS ONE* **10**, e0118571 (2015).

26. National Climate Change Secretariat. Impact Of Climate Change In Singapore. https://www.nccs.gov.sg/singapores-climate-action/impact-of-climate-change-in-singapore/ (2023).

27. Woodroffe, C. & McLean, R. Microatolls and recent sea level change on coral atolls. *Nature* **344**, 531–534 (1990).

28. Hanebuth, T., Stattegger, K. & Grootes, P. M. Rapid Flooding of the Sunda Shelf: A Late-Glacial Sea-Level Record. *Science* **288**, 1033–1035 (2000).

29. Michel, G. W., Becker, M., Angermann, D., Reigber, C. & Reinhart, E. Crustal motion in E-and SE-Asia from GPS measurements. *Earth Planet Sp* **52**, 713–720 (2000).

30. Simons, W. J. F. *et al.* A decade of GPS in Southeast Asia: Resolving Sundaland motion and boundaries. *J. Geophys. Res.* **112**, B06420 (2007).

31. Tjia, H. D. Sea-level changes in the tectonically stable Malay-Thai Peninsula. *Quaternary International* **31**, 95–101 (1996).

32. Dodd, T. J. H. *et al.* Paleozoic to Cenozoic sedimentary bedrock geology and lithostratigraphy of Singapore. *Journal of Asian Earth Sciences* **180**, 103878 (2019).

33. Leslie, A. G. *et al.* Ductile and brittle deformation in Singapore: A record of Mesozoic orogeny and amalgamation in Sundaland, and of post-orogenic faulting. *Journal of Asian Earth Sciences* **181**, 103890 (2019).

34. Chua, S. *et al.* A new Quaternary stratigraphy of the Kallang River Basin, Singapore: Implications for urban development and geotechnical engineering in Singapore. *Journal of Asian Earth Sciences* **200**, 104430 (2020).

35. Wiseman, K., Bürgmann, R., Freed, A. M. & Banerjee, P. Viscoelastic relaxation in a heterogeneous Earth following the 2004 Sumatra–Andaman earthquake. *Earth and Planetary Science Letters* **431**, 308–317 (2015).

36. Qiu, Q., Moore, J. D. P., Barbot, S., Feng, L. & Hill, E. M. Transient rheology of the Sumatran mantle wedge revealed by a decade of great earthquakes. *Nat Commun* **9**, 995 (2018).
37. Hu, Y. *et al.* Asthenosphere rheology inferred from observations of the 2012 Indian Ocean earthquake. *Nature* **538**, 368–372 (2016).
38. Kim, H. L. *et al.* Prehistoric human migration between Sundaland and South Asia was driven by sea-level rise. *Commun Biol* **6**, 1–10 (2023).
39. Jiwarungrueangkul, T., Liu, Z. & Zhao, Y. Terrigenous sediment input responding to sea level change and East Asian monsoon evolution since the last deglaciation in the southern South China Sea. *Global and Planetary Change* **174**, 127–137 (2019).
40. Shaw, T. A. *et al.* Deglacial perspectives of future sea level for Singapore. *Commun Earth Environ* **4**, 1–12 (2023).
41. Deschamps, P. *et al.* Ice-sheet collapse and sea-level rise at the Bølling warming 14,600 years ago. *Nature* **483**, 559–564 (2012).
42. Hanebuth, T. J. J., Voris, H. K., Yokoyama, Y., Saito, Y. & Okuno, J. Formation and fate of sedimentary depocentres on Southeast Asia's Sunda Shelf over the past sea-level cycle and biogeographic implications. *Earth-Science Reviews* **104**, 92–110 (2011).
43. Kamaludin, H. Holocene sea level changes in Peninsular Malaysia. *BGSM* **45**, 301–308 (2002).
44. Horton, B. P. *et al.* Holocene sea levels and palaeoenvironments, Malay-Thai Peninsula, southeast Asia. *The Holocene* **15**, 1199–1213 (2005).
45. Tan, F. *et al.* Holocene relative sea-level histories of far-field islands in the mid-Pacific. *Quaternary Science Reviews* **310**, 107995 (2023).

46. Caldwell, P. C., Merrifield, M. A. & Thompson, P. R. Sea level measured by tide gauges from global oceans — the Joint Archive for Sea Level holdings (NCEI Accession 0019568). (2015).

47. Horton, B. P., Edwards, R. J. & Lloyd, J. M. Implications of a microfossil-based transfer function in Holocene sea-level studies. **166**, 41–54 (2000).

48. Shennan, I. Handbook of sea-level research. in *Handbook of Sea-Level Research* 3–25 (John Wiley & Sons, Ltd, 2015). doi:10.1002/9781118452547.ch2.

49. Scoffin, T. P., Stoddart, D. R. & Rosen, B. R. The Nature and Significance of Microatolls. *Philosophical transactions of the Royal Society of London* **284**, 99–122 (1978).

50. Smithers, S. G. & Woodroffe, C. D. Microatolls as sea-level indicators on a mid-ocean atoll. *Marine Geology* **168**, 61–78 (2000).

51. Meltzner, A. J. *et al.* Half-metre sea-level fluctuations on centennial timescales from mid-Holocene corals of Southeast Asia. *Nat Commun* **8**, 14387 (2017).

52. Smithers, S. G. & Woodroffe, C. D. Coral microatolls and 20th century sea level in the eastern Indian Ocean. *Earth and Planetary Science Letters* **191**, 173–184 (2001).

53. Philibosian, B. *et al.* Rupture and variable coupling behavior of the Mentawai segment of the Sunda megathrust during the supercycle culmination of 1797 to 1833. *J. Geophys. Res. Solid Earth* **119**, 7258–7287 (2014).

54. Meltzner, A. J. *et al.* Coral evidence for earthquake recurrence and an A.D. 1390–1455 cluster at the south end of the 2004 Aceh–Andaman rupture. *J. Geophys. Res.* **115**, B10402 (2010).

55. Majewski, J. M. *et al.* Extending instrumental sea-level records using coral microatolls, an example from Southeast Asia. *Geophysical Research Letters* **49**, (2022).

56. Meltzner, A. J. & Woodroffe, C. D. Coral microatolls. in *Handbook of Sea-Level Research* 125–145 (John Wiley & Sons, Ltd, 2015). doi:10.1002/9781118452547.ch8.

57. Horton, B. P. *et al.* Predicting marsh vulnerability to sea-level rise using Holocene relative sea-level data. *Nat Commun* **9**, 2687 (2018).

58. Shennan, I., Tooley, M. J., Davis, M. J. & Haggart, B. A. Analysis and interpretation of Holocene sea-level data. *Nature* **302**, 404–406 (1983).

59. Mawdsley, R. J., Haigh, I. D. & Wells, N. C. Global secular changes in different tidal high water, low water and range levels. *Earth's Future* **3**, 66–81 (2015).

60. Pugh, D. & Woodworth, P. *Sea-Level Science: Understanding Tides, Surges, Tsunamis and Mean Sea-Level Changes*. (Cambridge University Press, 2014). doi:10.1017/CBO9781139235778.

61. Woodworth, P. L. Differences between mean tide level and mean sea level. *J Geod* **91**, 69–90 (2017).

62. Hyndman, R. J. Computing and Graphing Highest Density Regions. *The American Statistician* **50**, 120–126 (1996).

63. Majewski, J. M. *et al.* Holocene relative sea-level records from coral microatolls in Western Borneo, South China Sea. *The Holocene* **28**, 1431–1442 (2018).

64. Yu, K.-F., Zhao, J.-X., Done, T. & Chen, T.-G. Microatoll record for large century-scale sea-level fluctuations in the mid-Holocene. *Quat. Res.* **71**, 354–360 (2009).

65. Woodroffe, C. D., McGregor, H. V., Lambeck, K., Smithers, S. G. & Fink, D. Mid-Pacific microatolls record sea-level stability over the past 5000 yr. *Geology* **40**, 951–954 (2012).

66. Shennan, I. Flandrian sea-level changes in the Fenland. I: The geographical setting and evidence of relative sea-level changes. *J. Quaternary Sci.* **1**, 119–153 (1986).

67. *Sea-Level Research: A Manual for the Collection and Evaluation of Data*. (Springer Netherlands, Dordrecht, 1986). doi:10.1007/978-94-009-4215-8.
68. Smithers, S. Microatoll. in *Encyclopedia of Modern Coral Reefs* 691–696 (Springer, Dordrecht, 2011). doi:10.1007/978-90-481-2639-2_111.
69. Scoffin, T. P., Brown, B. E., Dunne, R. P. & Tissier, M. D. A. L. The Controls on Growth Form of Intertidal Massive Corals, Phuket, South Thailand. *PALAIOS* **12**, 237 (1997).
70. Piecuch, C. G., Kemp, A. C., Gebbie, G. & Meltzner, A. J. Climate did not drive Common Era Maldivian sea-level lowstands. *Nat. Geosci.* **14**, 273–275 (2021).
71. Hallmann, N. *et al.* Ice volume and climate changes from a 6000 year sea-level record in French Polynesia. *Nat Commun* **9**, 285 (2018).
72. Goodwin, I. D. & Harvey, N. Subtropical sea-level history from coral microatolls in the Southern Cook Islands, since 300 AD. *Marine Geology* **253**, 14–25 (2008).
73. Cahill, N., Kemp, A. C., Horton, B. P. & Parnell, A. C. Modeling sea-level change using errors-in-variables integrated Gaussian processes. *Ann. Appl. Stat.* **9**, 547–571 (2015).
74. *Generalized Linear Models: A Bayesian Perspective*. (CRC Press, Boca Raton, 2000). doi:10.1201/9781482293456.
75. Khan, N. S. *et al.* Inception of a global atlas of sea levels since the Last Glacial Maximum. *Quaternary Science Reviews* **220**, 359–371 (2019).
76. Reimer, P. J. *et al.* The IntCal20 Northern Hemisphere Radiocarbon Age Calibration Curve (0–55 cal kBP). *Radiocarbon* **62**, 725–757 (2020).
77. Heaton, T. J. *et al.* Marine20—The Marine Radiocarbon Age Calibration Curve (0–55,000 cal BP). *Radiocarbon* **62**, 779–820 (2020).

78. Peltier, W. R., Argus, D. F. & Drummond, R. Space geodesy constrains ice age terminal deglaciation: The global ICE-6G_C (VM5a) model. *J. Geophys. Res. Solid Earth* **120**, 450–487 (2015).

79. Li, T., Wu, P., Steffen, H. & Wang, H. In search of laterally heterogeneous viscosity models of glacial isostatic adjustment with the ICE-6G_C global ice history model. *Geophysical Journal International* **214**, 1191–1205 (2018).

80. Li, T. & Wu, P. Laterally heterogeneous lithosphere, asthenosphere and sub-lithospheric properties under Laurentia and Fennoscandia from Glacial Isostatic Adjustment. *Geophysical Journal International* **216**, 1633–1647 (2019).

81. Chutcharavan, P. M., Dutton, A. & Ellwood, M. J. Seawater 234U/238U recorded by modern and fossil corals. *Geochimica et Cosmochimica Acta* **224**, 1–17 (2018).

82. Bagnato, S., Linsley, B. K., Howe, S. S., Wellington, G. M. & Salinger, J. Evaluating the use of the massive coral *Diploastrea heliopora* for paleoclimate reconstruction: D. HELIOPORA PALEOCLIMATE RECONSTRUCTION. *Paleoceanography* **19**, PA1032 (2004).

83. Dassié, E. P. & Linsley, B. K. Refining the sampling approach for the massive coral Diploastrea heliopora for δ18O-based paleoclimate applications. *Palaeogeography, Palaeoclimatology, Palaeoecology* **440**, 274–282 (2015).

84. Watanabe, T. *et al.* Oxygen isotope systematics in Diploastrea heliopora: new coral archive of tropical paleoclimate. *Geochimica et Cosmochimica Acta* **67**, 1349–1358 (2003).

85. Lough, J. M. & Cantin, N. E. Perspectives on Massive Coral Growth Rates in a Changing Ocean. *The Biological Bulletin* **226**, 187–202 (2014).

86. Todd, P., Ladle, R., Lewin-Koh, N. & Chou, L. Genotype × environment interactions in transplanted clones of the massive corals Favia speciosa and Diploastrea heliopora. *Mar. Ecol. Prog. Ser.* **271**, 167–182 (2004).

87. Hennige, S. *et al.* Photoacclimation, growth and distribution of massive coral species in clear and turbid waters. *Mar. Ecol. Prog. Ser.* **369**, 77–88 (2008).

88. Damassa, T. D., Cole, J. E., Barnett, H. R., Ault, T. R. & McClanahan, T. R. Enhanced multidecadal climate variability in the seventeenth century from coral isotope records in the western Indian Ocean: SEVENTEENTH CENTURY MULTIDECADAL VARIABILITY. *Paleoceanography* **21**, PA2016 (2006).

89. Gopinadha Pillai, C. S. The distribution of Shallow-water Stony Corals at Minicoy Atoll in the Indian Ocean with a check-list of species. *Atoll Research Bulletin* **141**, (1971).

90. Kanisan, D. P. *et al.* Diversity and Distribution of Microbial Communities Associated with Reef Corals of the Malay Peninsula. *Microb Ecol* **85**, 37–48 (2023).

91. Schuhmacher, H., Loch, K., Loch, W. & See, W. R. The aftermath of coral bleaching on a Maldivian reef—a quantitative study. *Facies* **51**, 80–92 (2005).

92. Richards, Z. T., Beger, M., Pinca, S. & Wallace, C. C. Bikini Atoll coral biodiversity resilience five decades after nuclear testing. *Marine Pollution Bulletin* **56**, 503–515 (2008).

93. Li, X. *et al.* Coral community changes in response to a high sedimentation event: A case study in southern Hainan Island. *Chin. Sci. Bull.* **58**, 1028–1037 (2013).

94. Stafford-Smith, M. G. Sediment-rejection efficiency of 22 species of Australian scleractinian corals. *Marine Biology* **115**, 229–243 (1993).

95. Done, T. J. & Potts, D. C. Influences of habitat and natural disturbances on contributions of massive Porites corals to reef communities. *Marine Biology* **114**, 479–493 (1992).

96. Bird, M. I., Fifield, L. K., Chua, S. & Goh, B. Calculating Sediment Compaction for Radiocarbon Dating of Intertidal Sediments. *Radiocarbon* **46**, 421–435 (2004).

97. Brain, M. J. *et al.* Exploring mechanisms of compaction in salt-marsh sediments using Common Era relative sea-level reconstructions. *Quaternary Science Reviews* **167**, 96–111 (2017).

98. Tjia, H. D. Holocene sea-level changes in the Malay-Thai Peninsula, a tectonically stable environment. *BGSM* **31**, 157–176 (1992).

99. Bird, M. I. *et al.* An inflection in the rate of early mid-Holocene eustatic sea-level rise: A new sea-level curve from Singapore. *Estuarine, Coastal and Shelf Science* **71**, 523–536 (2007).

100. Hesp, P., Chang, C. H., Hilton, M., Chou, L. & Turner, I. M. A first tentative Holocene sea-level curve for Singapore. *Journal of Coastal Research* **14**, 308–314 (1998).

101. Meltzner, A. J. *et al.* Persistent termini of 2004- and 2005-like ruptures of the Sunda megathrust. *Journal of Geophysical Research: Solid Earth* **117**, B04405 (2012).

102. Philibosian, B. *et al.* Earthquake supercycles on the Mentawai segment of the Sunda megathrust in the seventeenth century and earlier. *Journal of Geophysical Research: Solid Earth* **122**, 642–676 (2017).

103. Weil-Accardo, J. *et al.* Two hundred thirty years of relative sea level changes due to climate and megathrust tectonics recorded in coral microatolls of Martinique (French West Indies): LESSER ANTILLES MICROATOLLS RECORD. *J. Geophys. Res. Solid Earth* **121**, 2873–2903 (2016).

104. Cobb, K. M., Charles, C. D., Cheng, H. & Edwards, R. L. El Niño/Southern Oscillation and tropical Pacific climate during the last millennium. *Nature* **424**, 271–276 (2003).

105. Murray-Wallace, C. V. & Woodroffe, C. D. Sea-level changes since the Last Glacial Maximum. in *Quaternary Sea-Level Changes: A Global Perspective* 320–368 (Cambridge University Press, 2014). doi:10.1017/CBO9781139024440.008.

106. Cobb, K. M., Charles, C. D., Cheng, H., Kastner, M. & Edwards, R. L. U/Th-dating living and young fossil corals from the central tropical Pacific. *Earth and Planetary Science Letters* **210**, 91–103 (2003).

107. Zhao, J., Yu, K. & Feng, Y. High-precision 238U–234U–230Th disequilibrium dating of the recent past: a review. *Quaternary Geochronology* **4**, 423–433 (2009).

108. Cantin, N. E., Cohen, A. L., Karnauskas, K. B., Tarrant, A. M. & McCorkle, D. C. Ocean Warming Slows Coral Growth in the Central Red Sea. *Science* **329**, 322–325 (2010).

109. Woodroffe, S. A. & Horton, B. P. Holocene sea-level changes in the Indo-Pacific. *Journal of Asian Earth Sciences* **25**, 29–43 (2005).

110. Clark, J. A., Farrell, W. E. & Peltier, W. R. Global Changes in Postglacial Sea Level: A Numerical Calculation. *Quat. Res.* **9**, 265–287 (1978).

111. Mitrovica, J. X. & Milne, G. A. On the origin of late Holocene sea-level highstands within equatorial ocean basins. *Quaternary Science Reviews* **21**, 2179–2190 (2002).

112. Roy, K. & Peltier, W. R. Space-geodetic and water level gauge constraints on continental uplift and tilting over North America: regional convergence of the ICE-6G_C (VM5a/VM6) models. *Geophysical Journal International* **210**, 1115–1142 (2017).

113. Peltier, W. R. Global glacial isostasy and the surface of the ice-age earth: the ICE-5G (VM2) model and GRACE. *Annual Review of Earth and Planetary Sciences* **32**, 111–149 (2004).

114. Badding, M. E., Briner, J. P. & Kaufman, D. S. 10Be ages of late Pleistocene deglaciation and Neoglaciation in the north-central Brooks Range, Arctic Alaska. *Journal of Quaternary Science* **28**, 95–102 (2013).

115. Crump, S. E., Anderson, L. S., Miller, G. H. & Anderson, R. S. Interpreting exposure ages from ice-cored moraines: a Neoglacial case study on Baffin Island, Arctic Canada. *Journal of Quaternary Science* **32**, 1049–1062 (2017).

116. Hall, B. L., Koffman, T. & Denton, G. H. Reduced ice extent on the western Antarctic Peninsula at 700–970 cal. yr B.P. *Geology* **39**, 635–638 (2010).

117. Kaplan, M. R. *et al.* Holocene glacier behavior around the northern Antarctic Peninsula and possible causes. *Earth and Planetary Science Letters* **534**, 116077 (2020).

118. Palacios, D. *et al.* Timing of formation of neoglacial landforms in the South Shetland Islands (Antarctic Peninsula): Regional and global implications. *Quaternary Science Reviews* **234**, 106248 (2020).

119. Zurbuchen, J. & Simms, A. R. Late Holocene ice-mass changes recorded in a relative sea-level record from Joinville Island, Antarctica. *Geology* **47**, 1064–1068 (2019).

120. Goodwin, I. D. Did changes in Antarctic ice volume influence Late Holocene sea-level lowering? *Quaternary Science Reviews* **17**, 319–332 (1998).

121. Jones, R. S. *et al.* Stability of the Antarctic Ice Sheet during the pre-industrial Holocene. *Nat Rev Earth Environ* **3**, 500–515 (2022).

122. Bird, M. I., Pang, W. C. & Lambeck, K. The age and origin of the Straits of Singapore. *Palaeogeography, Palaeoclimatology, Palaeoecology* **241**, 531–538 (2006).

123. Sarr, A.-C. *et al.* Subsiding Sundaland. *Geology* **47**, 119–122 (2019).

124. Tay, C. *et al.* Sea-level rise from land subsidence in major coastal cities. *Nat Sustain* **5**, 1049–1057 (2022).

125. Brain, M. J. *et al.* Modelling the effects of sediment compaction on salt marsh reconstructions of recent sea-level rise. *Earth and Planetary Science Letters* **345–348**, 180–193 (2012).

126. Hall, R. The palaeogeography of Sundaland and Wallacea since the Late Jurassic. *J Limnol* **72**, e1 (2013).

127. Tkalich, P., Vethamony, P., Luu, Q.-H. & Babu, M. T. Sea level trend and variability in the Singapore Strait. *Ocean Sci.* **9**, 293–300 (2013).

128. Komori, J. Coral Microatoll Growth Simulator. (2023).

Tables

Table 1. Ages and elevations of Siloso fossil corals. For details on the ^{230}Th ages, refer to Table S1 in the Supporting Information. HDR: highest density region.

Sample ID	Elevation of top of core (m SHD)	Sample depth (m)	^{230}Th age of dated sample (yr BP) (2σ) [a]	Extrapolated age of top of core (yr BP) (95% HDR)
SILO F3 OUT	-1.54	0.11	636 ± 3 [b]	633 ± 4
SILO F3 IN	-1.51	0.08	839 ± 3 [b]	836 ± 5
SILO F18 OUT	-1.33	0.09	1635 ± 7 [b]	1634 ± 7
SILO F18 IN	-1.40	0.16	1773 ± 5 [b]	1754 ± 16
SILO F18 CEN	-1.43	0.12	1837 ± 12 [b]	1807 ± 21
SILO F15 OUT	-1.54	0.06	1726 ± 6	1715 ± 13
SILO F15 MID	-1.50	0.14	1876 ± 6	1853 ± 26
SILO F15 IN	-1.49	0.09	1900 ± 7	1884 ± 18
SILO F2 OUT	-1.23	0.10	2087 ± 6	2072 ± 10
SILO F2 IN	-1.19	0.07	2685 ± 7 [b]	2669 ± 11
SILO F5	-1.22	0.08	2239 ± 7	2228 ± 10
SILO F1 OUT	-1.26	0.12	2578 ± 6 [b]	2570 ± 7
SILO F1 IN	-1.30	0.06	2731 ± 8	2729 ± 8
SILO F6	-1.20	0.07	2787 ± 9	2782 ± 10
SILO F7	-1.23	0.08	2812 ± 10	2805 ± 12

[a] *The ^{230}Th ages have been corrected for initial detrital Thorium assuming an ^{230}Th/^{232}Th atomic ratio of 4.4 ± 2.2 x 10^{-6}. Refer to Supporting Text S3 for details on the sensitivity test conducted on the assumed ^{230}Th/^{232}Th atomic ratio.*
[b] *Age here is the weighted mean age and standard error derived from subsamples of the same core.*

Table 2. Relative sea-level (RSL) from fossil Diploastrea heliopora corals at Siloso, Sentosa. Ages here are the modelled ages for the top of the core (refer to Table 1). HDR: highest density region.

Sample ID	Age (yr BP) (95% HDR)	Age (CE) (95% HDR)	RSL (m) (2σ)	Type
SILO F3 OUT	633 ± 4	1317 ± 4	-0.06 ± 0.13	sea-level index point
SILO F3 IN	836 ± 5	1114 ± 5	-0.03 ± 0.13	sea-level index point
SILO F18 OUT	1634 ± 7	316 ± 7	0.15 ± 0.13	sea-level index point

SILO F18 IN	1754 ± 16	196 ± 16	0.09 ± 0.13	sea-level index point
SILO F18 CEN	1807 ± 21	143 ± 21	0.05 ± 0.13	sea-level index point
SILO F15 OUT	1715 ± 13	235 ± 13	0.02 ± 0.16	sea-level index point
SILO F15 MID	1853 ± 26	97 ± 26	0.06 ± 0.16	sea-level index point
SILO F15 IN	1884 ± 18	66 ± 18	0.07 ± 0.16	sea-level index point
SILO F2 OUT	2072 ± 10	-122 ± 10	> 0.13	marine limiting
SILO F2 IN	2669 ± 11	-719 ± 11	> 0.17	marine limiting
SILO F5	2228 ± 10	-278 ± 10	> 0.14	marine limiting
SILO F1 OUT	2570 ± 7	-620 ± 7	0.23 ± 0.13	sea-level index point
SILO F1 IN	2729 ± 8	-779 ± 8	0.19 ± 0.13	sea-level index point
SILO F6	2782 ± 10	-832 ± 10	0.28 ± 0.13	sea-level index point
SILO F7	2805 ± 12	-855 ± 12	0.25 ± 0.13	sea-level index point

Legends

Figure 1. (a) Map of study region. The boundary of the Sunda Shelf is based on the 200 m bathymetric contour[126]. Bathymetry was made with Natural Earth. Tectonic faults (red) are based on Meltzner et al. (2012), Hinschberger et al. (2005) and Mendoza et al. (2022). (b) Map showing the location of Late Holocene data points in the existing Singapore RSL database (Chua et al., 2021), in relation to the Southern Islands. (c) Map of the Southern Islands, showing the location of Siloso in relation to the nearby sites of Semakau and Kusu Islands where living *Diploastrea heliopora* microatolls were surveyed (yellow-filled dots). Bathymetry in panels b and c are estimated from Tkalich et al. (2013) (d) Orthomosaic of the Siloso reef. Filled circles: locations of fossil corals in this study, coloured by age groups. Filled squares: locations of living *Porites* sp. microatolls. White-filled dot: portable tide gauge deployed in this study. LCK: Lim Chu Kang; SBU: Sungei Buloh; GEY: Geylang; SEK: Sekudu; KRB: Kallang River Basin. TJPG: Tanjong Pagar Tide Gauge, managed by the Maritime Port Authority of Singapore (MPA).

Figure 2. Coral microatoll growth tracks relative sea-level change. (a, b) Photographs of a living *Porites* sp. microatoll at Siloso, documented in year 2020 within 1-2 months of a ~7 cm diedown. (c - e) 3D schematic (top) and cross-sectional radial profiles (bottom) showing the coral microatoll HLG tracking (c) stable, (d) rising and (e) falling relative sea level. In panels c through e, we show only every 4th annual band of each radial cross section for clarity. Each black tic mark at the bottom of panels c – e represents a year. The blue curves (middle) show changes in the lowest annual tide from year to year and represents the theoretical HLS that the coral can grow up to. Each time the coral HLG catches up to the lowest tide, a diedown occurs (red dot). Consecutive diedowns occur in years when the lowest annual tides get progressively lower. For simplicity, we label each cluster of diedowns collectively as one diedown (numbered); in the radial cross sections (c - e, bottom panels), we show only the lowest diedown in each cluster of diedowns for clarity. These labelled diedown clusters are ~18.61 yrs apart and are modulated by the lunar nodal cycle[51]. HLS: highest level of survival; HLG: highest level of growth. 3D coral microatoll schematics in panels c-e were developed using the 3D coral microatoll simulator of Ref.[128].

Figure 3. Digital surface models of selected fossil coral microatolls. Digital surface models overlain on orthomosaics of (a) SILO F1, (b) SILO F3, (c) SILO F15 and (d) SILO F18. Concentric rings are labelled from the youngest (outermost) to oldest (innermost), beginning with ring 1 ('R1'); CEN: the inferred centre of the microatoll. Note that the ring labels are only internally consistent within each microatoll and rings with the same label do not indicate coeval features inferred across corals. In panel c, only the elevations of the ring crests of SILO F15 are accurate; the troughs between the ring crests are covered partially by water and refraction causes the elevations of the troughs to be inaccurate. Red lines: transects shown in Figure 4 (A-A',B-B',C-C',D-D'); dashed black lines: inferred ring boundaries; dashed white lines: coral microatoll boundary; shaded regions: inferred overgrowth; white points bordered in red: core locations. Red arrows in panels c and d indicate the inferred diedown that is common to both SILO F15 and SILO F18.

Figure 4. U-Th dates from coral cores are in sequence (ages become younger going radially outwards). Radial cross-sectional profiles of fossil *Diploastrea heliopora* coral microatolls SILO F1, SILO F3, SILO F15 and SILO F18, indicating position of cores (hollow rectangles) and sample depths that were subsampled for dating (black rectangles). Blue numbers: U-Th ages (yrs BP). BP: "Before Present", where present refers to the year 1950 CE. The "IN" and "OUT" cores in each microatoll (excluding those marked with an *; see Table 1) were used to scale each fossil coral microatoll from horizontal distance to age, to produce the cross-sectional profiles in Figure 5B. Note that all four microatolls have been scaled to the same vertical and horizontal scales, and that the elevations are true to the y-axis, but the corals are not horizontally positioned in any given order.

Figure 5. RSL record from fossil corals at Siloso, Sentosa, Singapore. (a) Sea-level index points (SLIPs) and marine limiting data points colour coded by coral. Yellow rectangles indicate the indicative range (2σ) of the living highest level of growth (HLG) measured and estimated accordingly for living *Porites* sp. and *Diploastrea heliopora* coral microatolls at Siloso, Sentosa, between 2020 and 2022. The horizontal line of the marine limiting data points are plotted at the bottom of the RSL uncertainty and indicate that RSL could have been anywhere at or above the horizontal line; the vertical tick marks are only symbolic and their lengths do not represent RSL uncertainty. (b) Radial cross-sectional profiles extracted from digital surface models (Figures 3 & 4) and superimposed onto the SLIPs (coloured shaded boxes) for the dated cores. The cross-sectional profiles can be translated vertically and horizontally, but the position of each core (circle) must lie within its modelled age and elevation uncertainties (indicated by the bounds of the corresponding SLIP). For SILO F15, only the elevations of the ring crests are accurate; the troughs between the ring crests are partially submerged under water and the elevation model in these parts are inaccurate. (c) Direction of RSL change inferred from coral microatoll surface morphologies as sea-level tendencies (solid arrows) or from the relative elevations of successive SLIPs (dashed arrows). Shaded vertical grey bars

and corresponding numbered labels (1, 2 and 3) indicate the three distinct periods when sea-level tendencies were inferred. RSL: relative sea level.

Figure 6. Magnitude and rates of RSL change compared to glacial isostatic adjustment models. (a) Magnitude of RSL and (b) rates of RSL change from fossil corals at Siloso, Sentosa, Singapore (blue). Grey curves indicate the mean, 1σ and 2σ range of the Errors-In-Variables Integrated Gaussian Process (EIV-IGP) model predictions (Cahill et al., 2015). In panel b, the lower uncertainties at times corresponding to data gaps are an artifact of the model. (c) RSL data from Siloso compared to an ensemble of GIA model predictions[17]. The GIA model ensemble encompasses a variety of upper mantle (UM) and lower mantle (LM) viscosities, as well as ice-melting histories (global 1 kyr delay; 1 kyr delay in ice melting from Antarctica), modified with reference to the ICE-6G_C (VM5a) model[78]. Individual lines show selected GIA model predictions; the grey shaded wedge shows the 95th-percent credible interval of the GIA model ensemble predictions. Rectangles: sea-level index points; T-shaped symbols: marine limiting data. The horizontal line of the T-shaped symbols is plotted at the bottom of the RSL uncertainty and indicate that RSL could have been anywhere at or above the horizontal line. The age axis is in years 'before present' (BP), where 'present' refers to the year 1950 CE.RSL: relative sea level.

Figure 7. (a) Map of the study area showing the location of major faults (Meltzner et al., 2012; Hinschberger et al., 2005) and existing studies of Late Holocene RSL in the region (b,c) (locations 1 – 9). 1: Natuna Island (Wan et al., 2020); 2: Thale Noi, Thailand[44]; 3: Merang, Terengganu[9,11]; 4: Kuantan (Zhang et al., 2021); 5: Tioman[20]; 6: Singapore[18,99,100]; 7: Senggarang[19]; 8: Pasir Panjang, Malaysia[19]; 9: Port Dickson[19]; 10: Teluk Batik[98]; 11: Langkawi[98]. The boundary of the Sunda Shelf (dashed line) is based on the 200 m bathymetric contour[126]. Background: map of the ICE-6G_C HetML140 glacial isostatic adjustment model at 2 kyrs BP. (b) Holocene RSL data points for Singapore (site 6) compared to existing data from East Coast Malay Peninsula and Riau Islands (sites 1-5) and (c) West Coast Malay Peninsula (sites 7-11). Dashed lines: low quality data; solid fill: high quality data. The horizontal line of the T-shaped symbols is plotted at the bottom of the RSL uncertainty and indicate that RSL could have been anywhere at or above the horizontal line. The vertical ticks in the limiting data are purely symbolic and do not represent the magnitude of RSL uncertainty. RSL: relative sea level; SLIP: sea-level index point.

Table 1. Ages and elevations of Siloso fossil corals. For details on the ^{230}Th ages, refer to Table S1 in the Supporting Information. HDR: highest density region.

Table 2. Relative sea level (RSL) from fossil *Diploastrea heliopora* corals at Siloso, Sentosa. Ages here are the modelled ages for the top of the core (refer to Table 1). HDR: highest density region.

Figures

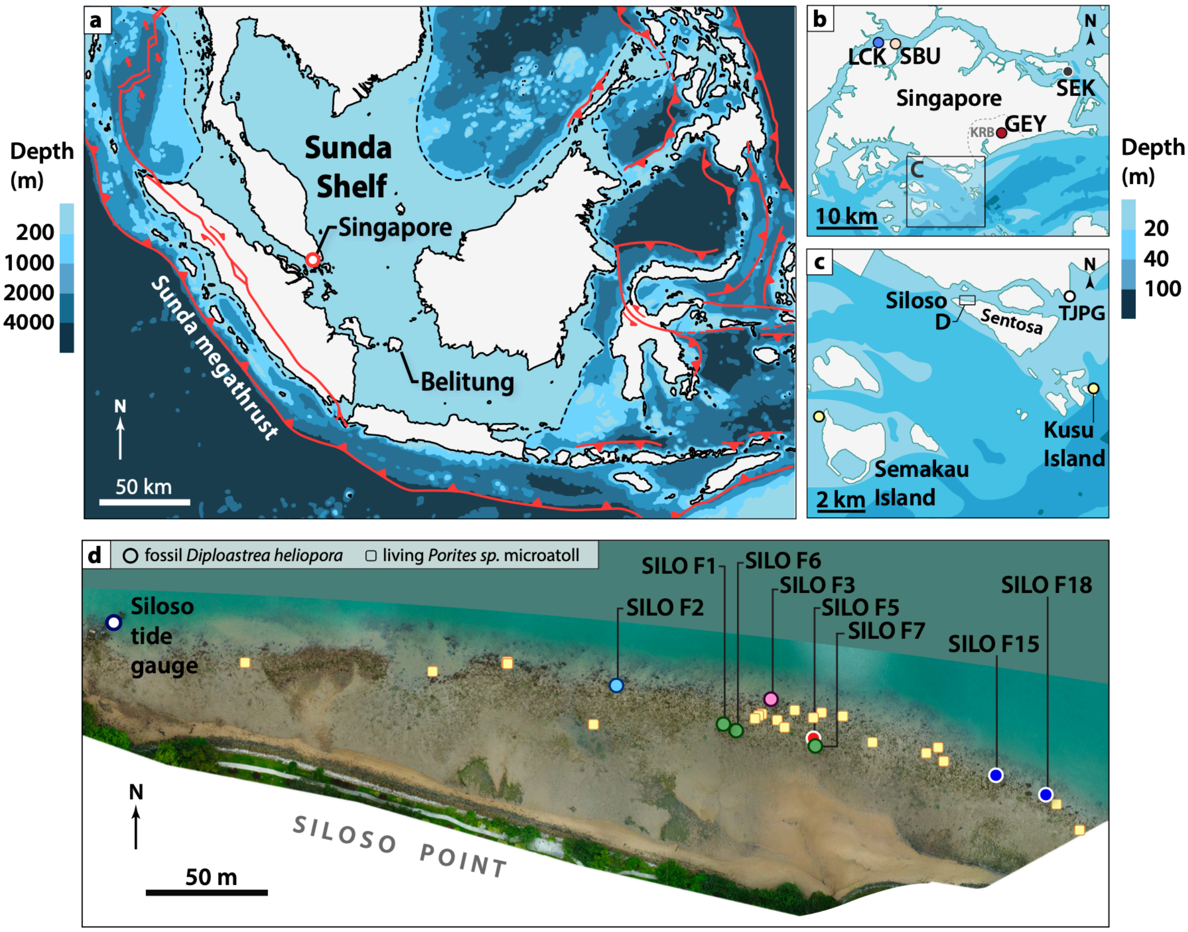

Figure 1. (a) Map of study region. The boundary of the Sunda Shelf is based on the 200 m bathymetric contour (Hall, 2013). Bathymetry was made with Natural Earth. Tectonic faults (red) are based on Meltzner et al. (2012), Hinschberger et al. (2005) and Mendoza et al. (2022). (b) Map showing the location of Late Holocene data points in the existing Singapore RSL database (Chua et al., 2021), in relation to the Southern Islands. (c) Map of the Southern Islands, showing the location of Siloso in relation to the nearby sites of Semakau and Kusu Islands where living *Diploastrea heliopora* microatolls were surveyed (yellow-filled dots). Bathymetry in panels b and c are estimated from Tkalich et al. (2013) (d) Orthomosaic of the Siloso reef. Filled circles: locations of fossil corals in this study, coloured by age groups. Filled squares: locations of living *Porites sp.* microatolls. White-filled dot: portable tide gauge deployed in this study. LCK: Lim Chu Kang; SBU: Sungei Buloh; GEY: Geylang; SEK: Sekudu; KRB: Kallang River Basin. TJPG: Tanjong Pagar Tide Gauge, managed by the Maritime Port Authority of Singapore (MPA).

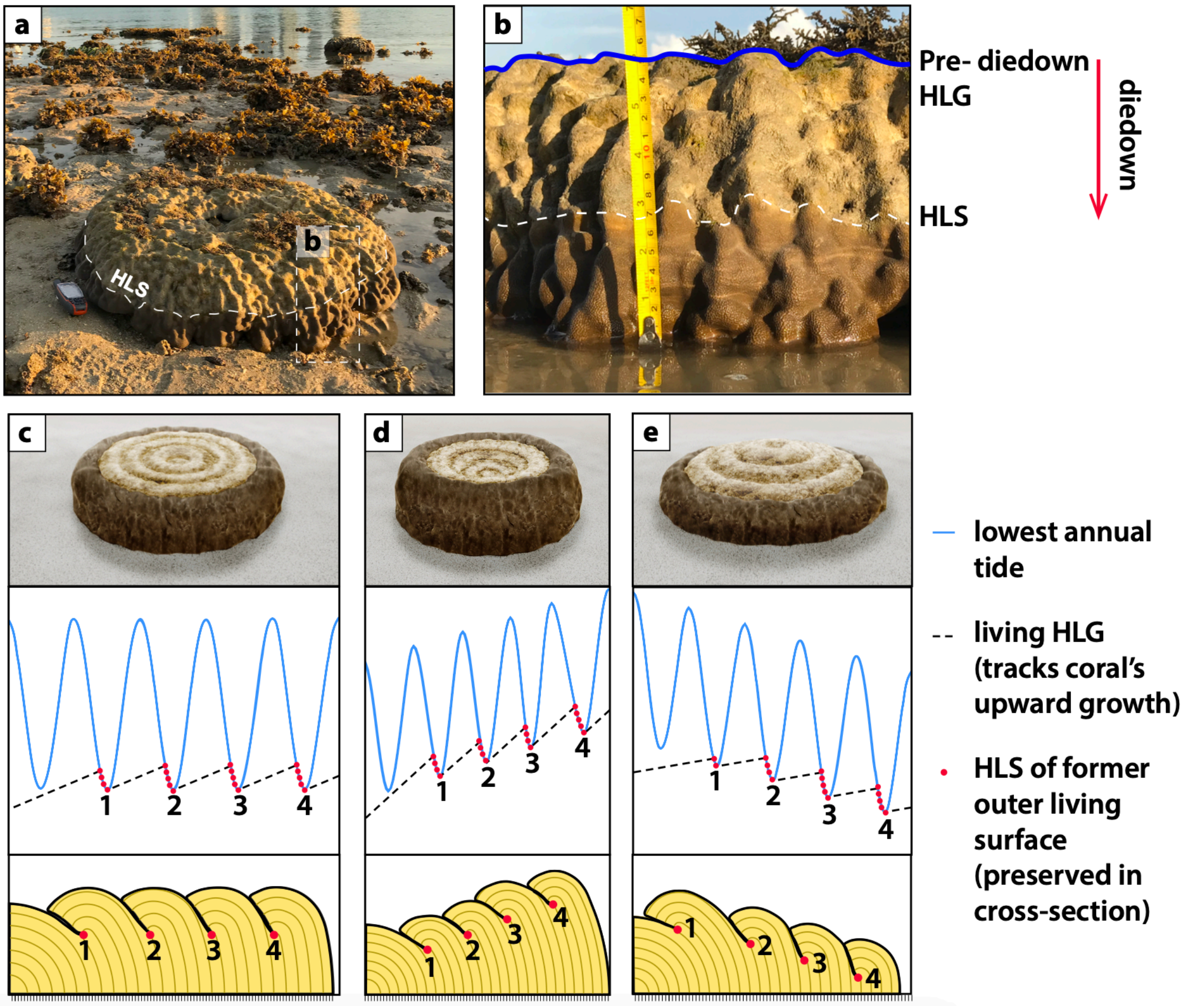

Figure 2. Coral microatoll growth tracks relative sea-level change. (a, b) Photographs of a living *Porites sp.* microatoll at Siloso, documented in year 2020 within 1-2 months of a ~7 cm diedown. (c - e) 3D schematic (top) and cross-sectional radial profiles (bottom) showing the coral microatoll HLG tracking (c) stable, (d) rising and (e) falling relative sea level. In panels c through e, we show only every 4th annual band of each radial cross section for clarity. Each black tic mark at the bottom of panels c – e represents a year. The blue curves (middle) show changes in the lowest annual tide from year to year and represents the theoretical HLS that the coral can grow up to. Each time the coral HLG catches up to the lowest tide, a diedown occurs (red dot). Consecutive diedowns occur in years when the lowest annual tides get progressively lower. For simplicity, we label each cluster of diedowns collectively as one diedown (numbered); in the radial cross sections (c - e, bottom panels), we show only the lowest diedown in each cluster of diedowns for clarity. These labelled diedown clusters are ~18.61 yrs apart and are modulated by the lunar nodal cycle (Meltzner et al., 2017). HLS: highest level of survival; HLG: highest level of growth. 3D coral microatoll schematics in panels c-e were developed using the 3D coral microatoll simulator of Ref.(Komori, 2023).

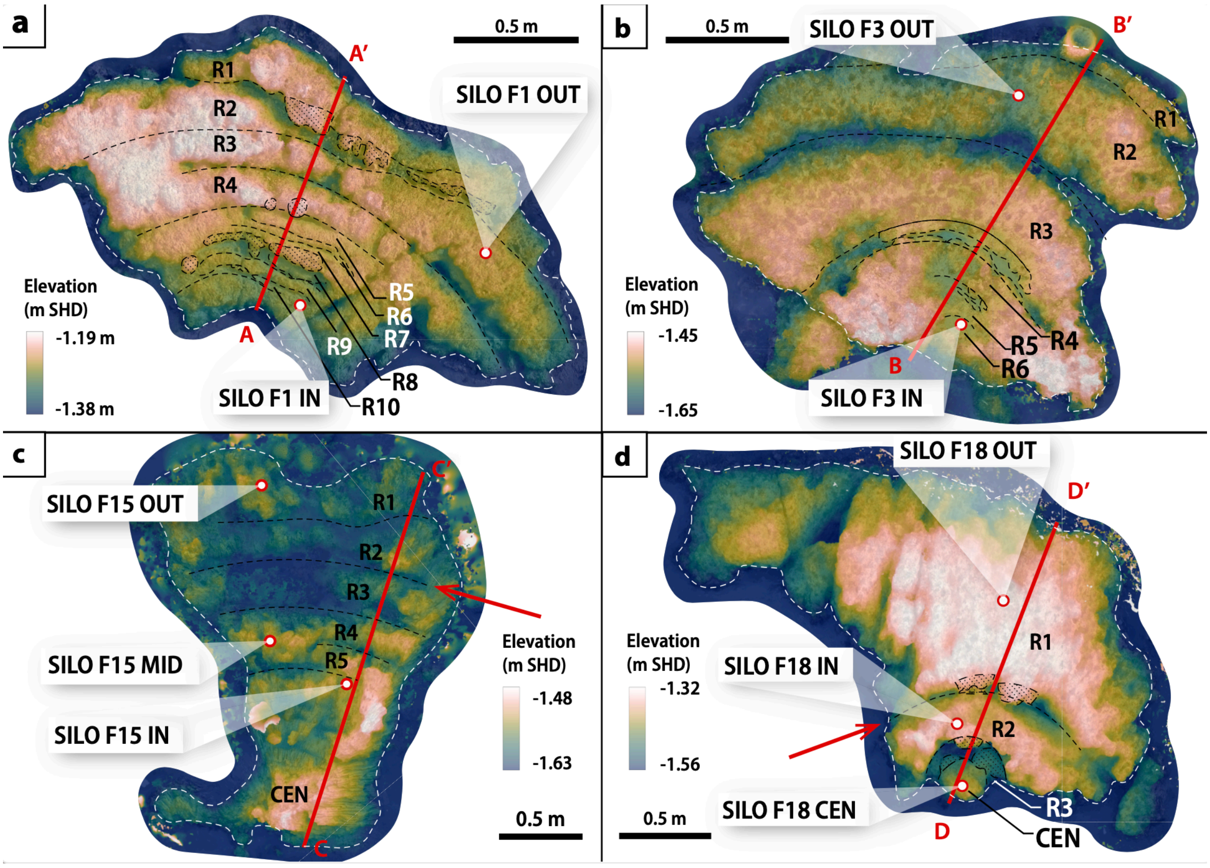

Figure 3. Digital surface models of selected fossil coral microatolls. Digital surface models overlain on orthomosaics of (a) SILO F1, (b) SILO F3, (c) SILO F15 and (d) SILO F18. Concentric rings are labelled from the youngest (outermost) to oldest (innermost), beginning with ring 1 ('R1'); CEN: the inferred centre of the microatoll. Note that the ring labels are only internally consistent within each microatoll and rings with the same label do not indicate coeval features inferred across corals. In panel c, only the elevations of the ring crests of SILO F15 are accurate; the troughs between the ring crests are covered partially by water and refraction causes the elevations of the troughs to be inaccurate. Red lines: transects shown in Figure 4 (A-A',B-B',C-C',D-D'); dashed black lines: inferred ring boundaries; dashed white lines: coral microatoll boundary; shaded regions: inferred overgrowth; white points bordered in red: core locations. Red arrows in panels c and d indicate the inferred diedown that is common to both SILO F15 and SILO F18.

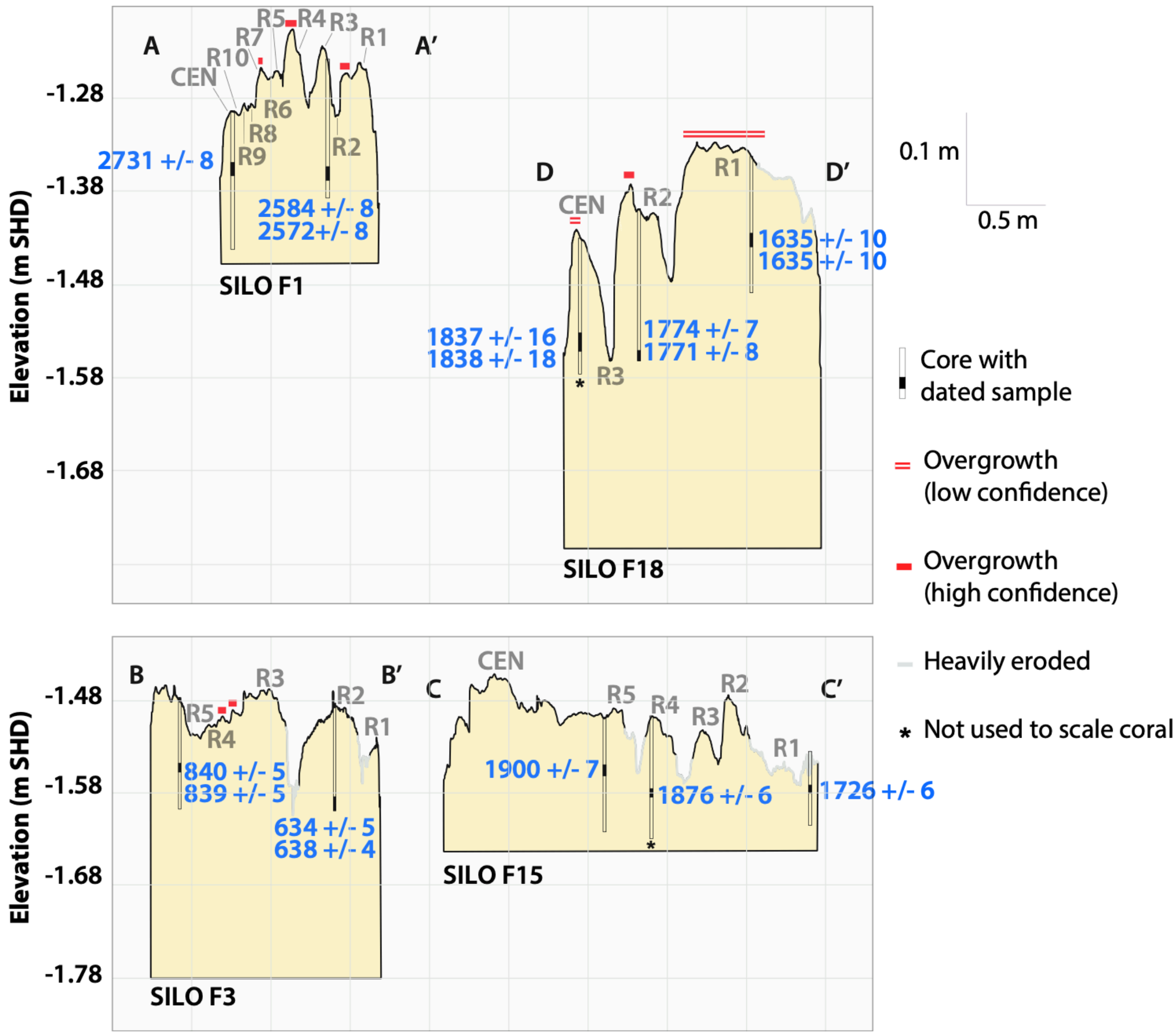

Figure 4. Cross-sectional profiles of fossil *Diploastrea heliopora* coral microatolls SILO F1, SILO F3, SILO F15 and SILO F18, indicating position of cores (hollow rectangles) and sample depths that were subsampled for dating (black rectangles). Blue numbers: U-Th ages (yrs BP). BP: "Before Present", where present refers to the year 1950 CE. The "IN" and "OUT" cores in each microatoll (excluding those marked with an *; see Table 1) were used to scale each fossil coral microatoll from horizontal distance to age, to produce the cross-sectional profiles in Figure 5B. Note that all four microatolls have been scaled to the same vertical and horizontal scales, and that the elevations are true to the y-axis, but the corals are not horizontally positioned in any given order.

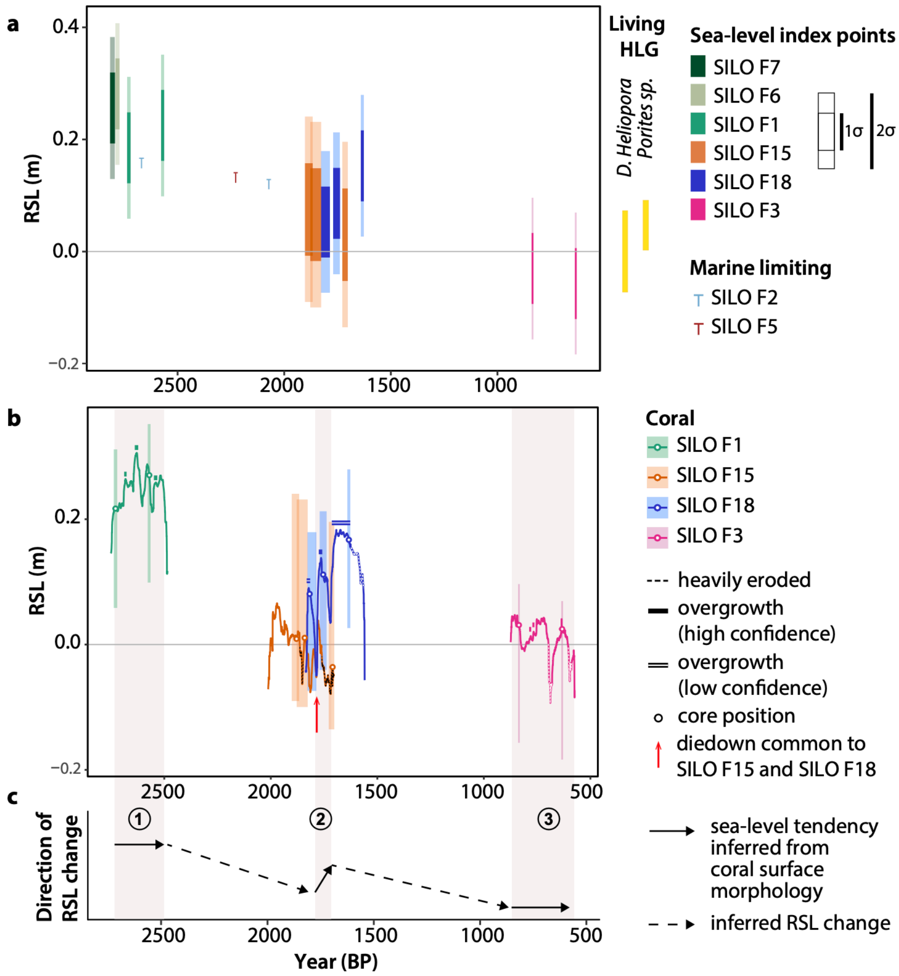

Figure 5. RSL record from fossil corals at Siloso, Sentosa, Singapore. (a) Sea-level index points (SLIPs) and marine limiting data points colour coded by coral. Yellow rectangles indicate the indicative range (2σ) of the living highest level of growth (HLG) measured and estimated accordingly for living *Porites sp.* and *Diploastrea heliopora* coral microatolls at Siloso, Sentosa, between 2020 and 2022. The horizontal line of the marine limiting data points are plotted at the bottom of the RSL uncertainty and indicate that RSL could have been anywhere at or above the horizontal line; the vertical tick marks are only symbolic and their lengths do not represent RSL uncertainty. (b) Radial cross-sectional profiles extracted from digital surface models (Figures 3 & 4) and superimposed onto the SLIPs (coloured shaded boxes) for the dated cores. The cross-sectional profiles can be translated vertically and horizontally, but the position of each core (circle) must lie within its modelled age and elevation uncertainties (indicated by the bounds of the corresponding SLIP). For SILO F15, only the elevations of the ring crests are accurate; the troughs between the ring crests are partially submerged under water and the elevation model in these parts are inaccurate. (c) Direction of RSL change inferred from coral microatoll surface morphologies as sea-level tendencies (solid arrows) or from the relative elevations of successive SLIPs (dashed arrows). Shaded vertical grey bars and corresponding numbered labels (1, 2 and 3) indicate the three distinct periods when sea-level tendencies were inferred. RSL: relative sea level.

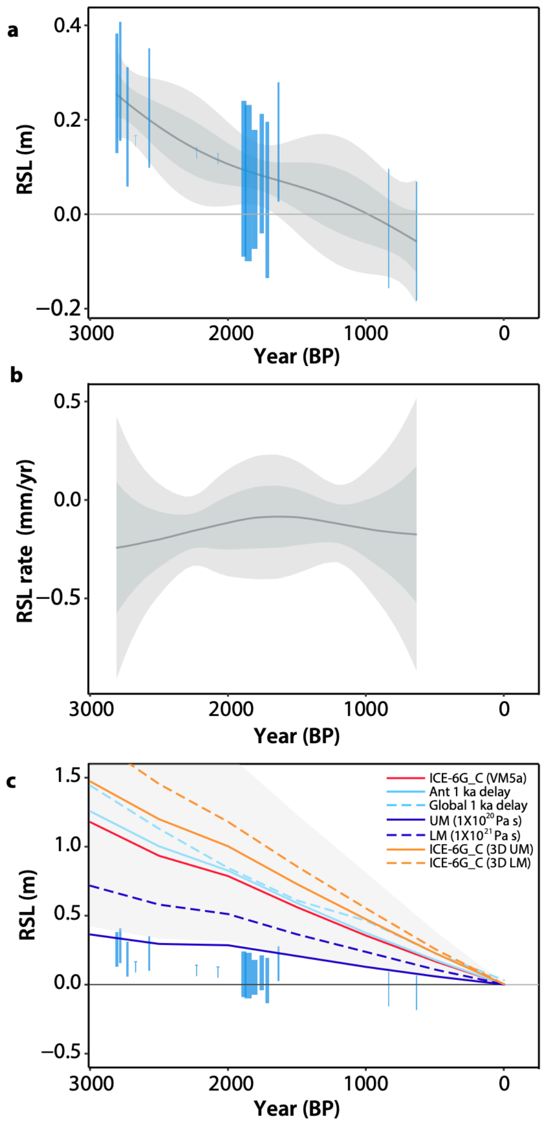

Figure 6. (a) Magnitude of RSL and (b) rates of RSL change from fossil corals at Siloso, Sentosa, Singapore (blue). Grey curves indicate the mean, 1σ and 2σ range of the Errors-In-Variables Integrated Gaussian Process (EIV-IGP) model predictions (Cahill et al., 2015). In panel b, the lower uncertainties at times corresponding to data gaps are an artifact of the model. (c) RSL data from Siloso compared to an ensemble of GIA model predictions (Li et al., 2023). The GIA model ensemble encompasses a variety of upper mantle (UM) and lower mantle (LM) viscosities, as well as ice-melting histories (global 1 kyr delay; 1 kyr delay in ice melting from Antarctica), modified with reference to the ICE-6G_C (VM5a) model (Peltier et al., 2015). Individual lines show selected GIA model predictions; the grey shaded wedge shows the 95th-percent credible interval of the GIA model ensemble predictions. Rectangles: sea-level index points; T-shaped symbols: marine limiting data. The horizontal line of the T-shaped symbols is plotted at the bottom of the RSL uncertainty and indicate that RSL could have been anywhere at or above the horizontal line. The age axis is in years 'before present' (BP), where 'present' refers to the year 1950 CE.RSL: relative sea level.

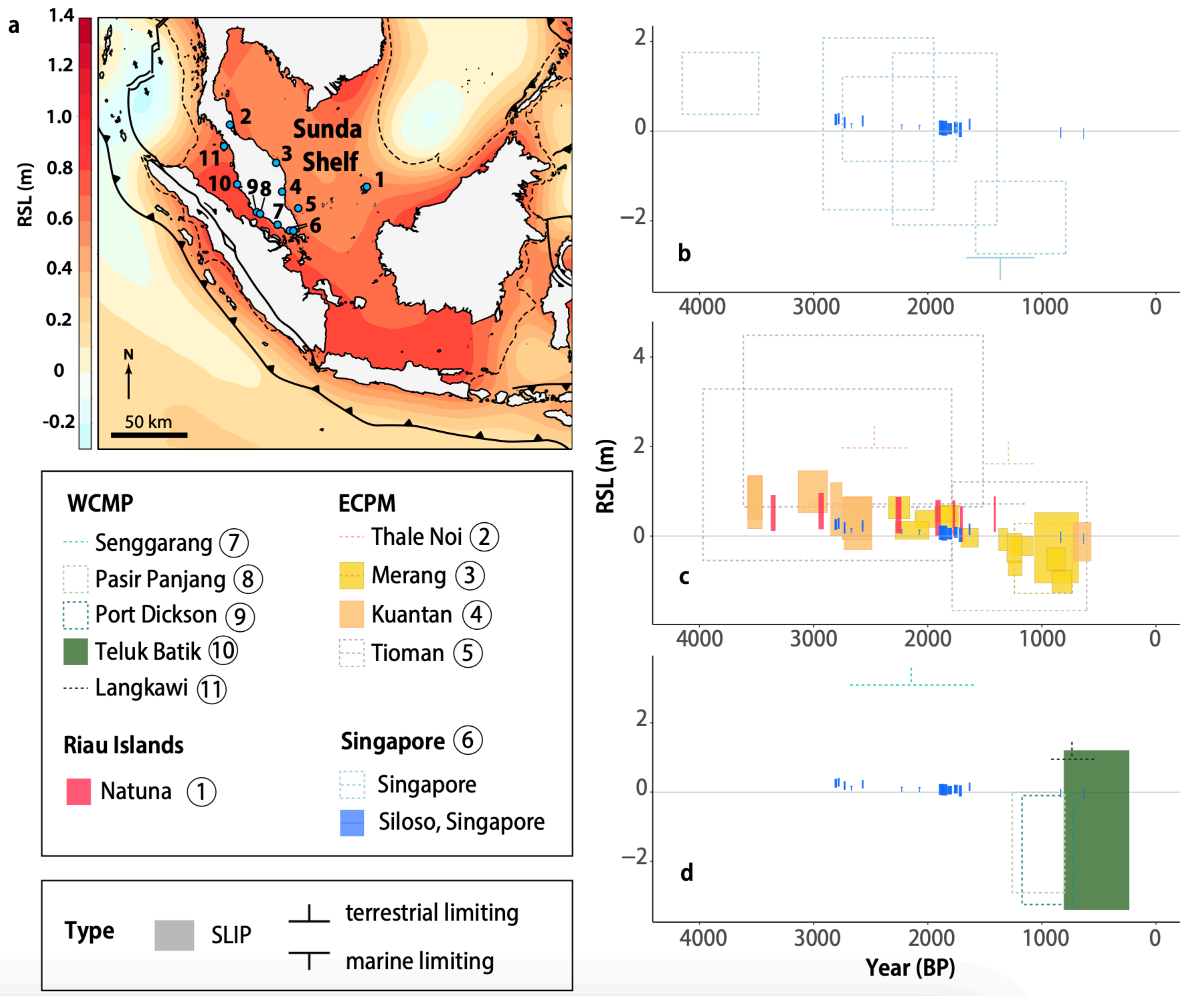

Figure 7. (a) Map of the study area showing the location of major faults (Meltzner et al., 2012; Hinschberger et al., 2005) and existing studies of Late Holocene RSL in the region (b,c) (locations 1 – 9). 1: Natuna Island (Wan et al., 2020); 2: Thale Noi, Thailand (Horton et al., 2005); 3: Merang, Terengganu (Kamaludin et al., 2016; Tam et al., 2018); 4: Kuantan (Zhang et al., 2021); 5: Tioman (Tjia et al., 1983); 6: Singapore (Bird et al., 2010, 2007; Hesp et al., 1998); 7: Senggarang (Geyh et al., 1979); 8: Pasir Panjang, Malaysia (Geyh et al., 1979); 9: Port Dickson (Geyh et al., 1979); 10: Teluk Batik (Tjia, 1992); 11: Langkawi (Tjia, 1992). The boundary of the Sunda Shelf (dashed line) is based on the 200 m bathymetric contour (Hall, 2013). Background: map of the ICE-6G_C HetML140 glacial isostatic adjustment model at 2 kyrs BP. (b) Holocene RSL data points for Singapore (site 6) compared to existing data from East Coast Malay Peninsula and Riau Islands (sites 1-5) and (c) West Coast Malay Peninsula (sites 7-11). Dashed lines: low quality data; solid fill: high quality data. The horizontal line of the T-shaped symbols is plotted at the bottom of the RSL uncertainty and indicate that RSL could have been anywhere at or above the horizontal line. The vertical ticks in the limiting data are purely symbolic and do not represent the magnitude of RSL uncertainty. RSL: relative sea level; SLIP: sea-level index point.